Universiteit Utrecht

Faculteit
Bètawetenschappen

Strongly Non-Linear Pressure-Induced Ion Currents in Conical Nanopores

Bachelor Thesis

Tim Elias Veenstra

Natuur- en Sterrenkunde

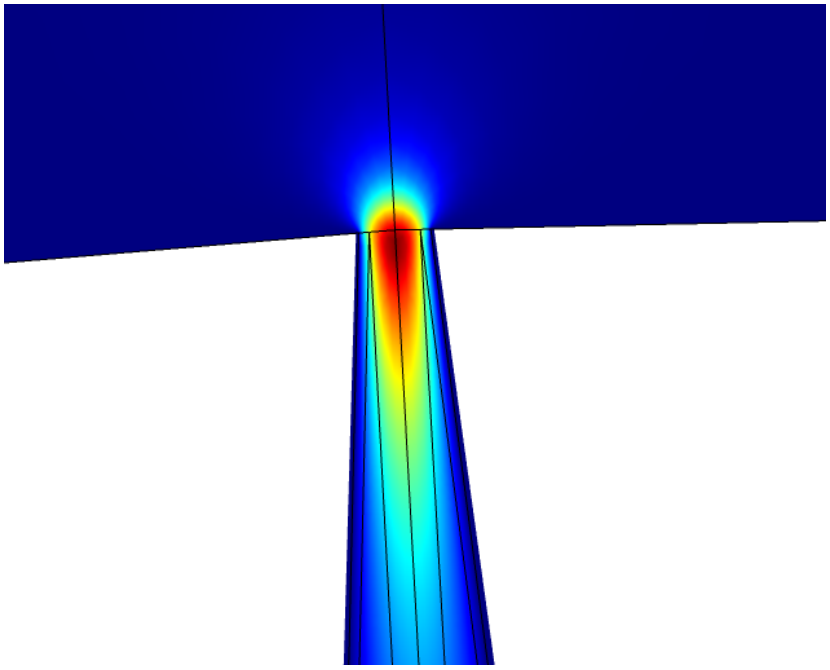

Supervisors:

Willem Boon, MSc Supervisor
Institute for Theoretical Physics

Prof Dr. René van Roij Supervisor
Institute for Theoretical Physics

June 12, 2020

Abstract

This research project investigates the non-linear behavior of pressure-induced currents in conical nanopores under influence of hydraulic and electric driving. This was hypothesized to be caused by space charge outside of the electric double layer. Numerical calculations were done to investigate the source of this non-linearity. Our data, however, point towards the conduction current as the cause of this transistor-like behavior, which is not related to charge inside the cone. We developed an analytical theory, based on a Poisson-Boltzmann framework for the electric double layer, to describe the salt concentration profile in the channel, which is directly related to the conduction current. A salt flux caused by a pressure difference counteracts the depletion or accumulation of salt in the channel. We conclude that this influence of the pressure on the concentration profile fully explains the observed current response.

Contents

1 Introduction

The transport of ions plays an important role in a host of biological processes, ranging from neuron activity to blood filtering. Therefore it should come as no surprise that organisms have developed complex mechanisms for the transportation of ions. For instance, cells contain ion channels that can pump ions against a concentration gradient [1], or ion channels that only open under mechanical stress or an applied electric field. [2] However, ion transport is not only important in biological systems, it is also used in nanotechnology and microfluidic devices. [3] For instance, a lot of research has been conducted during the last few decades on generating power with nanochannel membranes that can extract energy from mixing fresh and salt water, thus potentially providing a clean reliable energy source. [4–6]. This and many other possible applications make a theoretical understanding of ion transport of great importance.

Most of the interesting properties of ion transport in small systems like nano-channels stem from the fact that a layer of charge surrounds the walls of the channel. This layer of charge is called the electric double layer, or EDL for short. [7] This is mostly noticeable in channels with radii in the range of nanometers or micrometers, where the area-to-volume ratio is relatively high. This layer is caused by a surface charge on the wall which in turn is caused by the dissociation of charged ions. Water has a relatively high dielectric constant, which can cause molecule groups to 'break off' from the channel wall, leaving behind a net charge. This charge on the wall attracts oppositely charged ions and repels charge with like charge. This results in a region with a net charge when this wall is in contact with a salt solution, as is sketched in figure 1.

When a certain force is applied to such a system, some form of transport or flux is expected to occur. When you apply more pressure on the fluid at one end of the channel than on the other end, then a fluid flow will occur, proportional to the pressure difference. When you apply an electric field across the channel, then ions will start to move and create a conduction current proportional to the electric field. These linear relations are called Darcy's and Ohm's laws, respectively. [7] A fluid flow will also cause a current since the charge in the EDL will start to move with the fluid, causing a streaming current, and an electric field will also cause a fluid flow since moving ions will 'drag' the water along. In a straight cylindrical channel, these fluxes will all be linear in the driving force, *i.e.* doubling the driving force will double the flux. However, a paper from Jubin *et al.* reported a phenomenon in a conical nanopore where the current was very non-linear as a function of the pressure if an electric field was applied on top of the pressure drop. [8] For small pressure differences the current would increase dramatically for about the first 50mbar, just to flatten and return to a linear relationship for larger pressure differences. This behavior is remarkable and mimics a transistor-like functionality, where the conductivity of the channel is strongly dependent on an external stimulus: here the electric field.

Jubin *et al.* propose an explanation in terms of what they call Spatially Charged Zones (SCZ), an unexplained charge in the channel, that would yield the experimentally determined current response. There are, however,

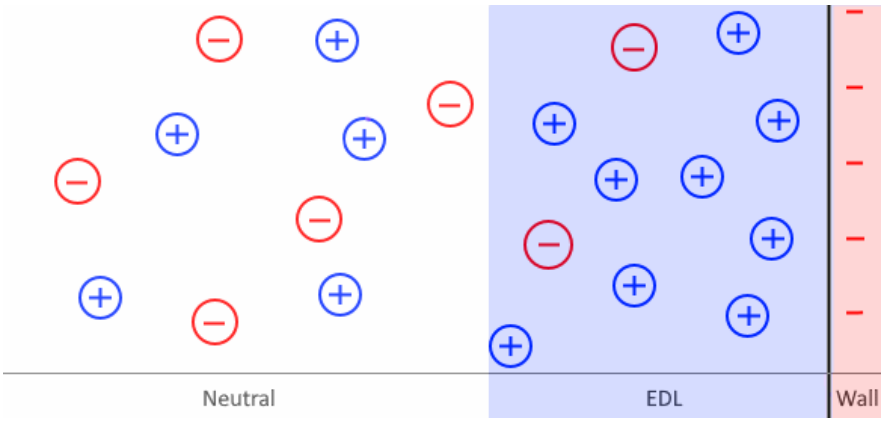

Figure 1: Sketch of the electric double layer (EDL) near a charged wall.

still some unanswered questions as to what causes these SCZs, and how exactly they would yield this specific current response. In this thesis we aim to show from first principles how the conductivity of the channel depends on a combination of electrical and mechanical driving forces. In order do this we will solve the governing set of equations for a cylindrical channel, both analytically and numerically. Then we will solve the conical system numerically and attempt to extend the theory to conical nanopores.

2 Electrostatics in Fluids

Now that the topic of this thesis has been introduced, let us take a look at the electrostatics of a simple system in equilibrium. In this section we will largely follow the derivations in section 8.2 of Ref. [7] and section 11.4 of Ref. [9]. We will however use SI units instead of Gaussian units, as they may be more intuitive and are easier to use in our numerical calculations. We consider a wall with a surface charge density $e\sigma$, which we assume is fixed. The wall is in contact with a salt solution which contains two monovalent ion species with opposite charge $\pm e$, which we will treat as point charges. We define the wall to be at $z = 0$ such that the solution is located in the space $z > 0$.

Derivation of Charge Distribution We are interested in the concentration profiles $\rho_\pm(z)$ of the positively and negatively charged ions, and the electrical potential $\psi(z)$, so we will need three equations to describe our system. The first one is the Poisson equation, given by

$$\nabla^2\psi = -\frac{eQ}{\varepsilon_0\varepsilon_r}, \tag{1}$$

where the charge density eQ is given by $eQ = e(\rho_+ - \rho_-)$ and ε_0 and ε_r are the vacuum permittivity and relative permittivity respectively. We assume the system is uniform in the x and y-directions, such that the Poisson equation reduces to

$$\frac{\partial^2\psi}{\partial z^2} = -\frac{e}{\varepsilon_0\varepsilon_r}\left(\rho_+(z) - \rho_-(z)\right). \tag{2}$$

The ionic density profiles can be described by a Boltzmann distribution where the energy of an ion with charge $\pm e$ is approximated by $\pm e\psi(z)$. The distribution then becomes

$$\rho_\pm = \rho_s \exp\{\mp\beta e\psi(z)\}, \tag{3}$$

where here ρ_s is the bulk concentration, for now, of both ion species and $\beta = 1/k_BT$. Equation 2 and 3 combined form the Poisson-Boltzmann equation:

$$\frac{\partial^2\psi}{\partial z^2} = -\frac{e\rho_s}{\varepsilon_0\varepsilon_r}\left(\exp[-e\beta\psi(z)] - \exp[+e\beta\psi(z)]\right) = \frac{2e\rho_s}{\varepsilon_0\varepsilon_r}\sinh(+e\beta\psi(z)). \tag{4}$$

We also need two boundary conditions to find a unique solution to our second order differential equation. First of all, we require the potential to be zero far from the wall, i.e.

$$\lim_{z\to\infty}\psi(z) = 0. \tag{5}$$

Secondly, we require electroneutrality if our system is in equilibrium. That is, the total ionic charge density and the surface charge density should cancel each other, which implies

$$e\sigma = -\int_0^\infty dz(eQ(z)) = \varepsilon_0\varepsilon_r\int_0^\infty dz\left(\frac{\partial^2}{\partial z^2}\psi(z)\right). \tag{6}$$

Using the fact that $\lim_{z\to\infty} d\psi(z)/dz = 0$, (which must be the case since we have already seen that $\lim_{z\to\infty}\psi(z) = 0$) we can write

$$\sigma = \frac{\varepsilon_0\varepsilon_r}{e}\left.\frac{\partial\psi}{\partial z}\right|_{z=0^+}. \tag{7}$$

For convenience, let us write the differential equation, equation 4, and its boundary conditions, equations 5 and 7 in terms of a non-dimensional potential $\phi(z) = \frac{e}{k_BT}\psi(z)$. We get

$$\begin{cases} \frac{\partial^2\phi(z)}{\partial z^2} = \kappa^2\sinh\{\phi(z)\}; \\ \frac{\partial\phi(0^+)}{\partial z} = -4\pi\lambda_B\sigma; \\ \lim_{z\to\infty}\phi(z) = 0, \end{cases} \tag{8}$$

where we have defined two length scales λ_B and κ^{-1} as

$$\kappa^{-1} = \left(\frac{2e^2\rho_s\beta}{\varepsilon_0\varepsilon_r}\right)^{-1/2}, \tag{9}$$

$$\lambda_B = \frac{e^2\beta}{4\pi\varepsilon_0\varepsilon_r}. \tag{10}$$

These are called the Debye (in some literature and in this thesis often denoted as λ_D) and Bjerrum lengths respectively. The set of equations from equation 2 can be solved analytically in this geometry [10]. The solution is

$$\phi(z) = 2\log\left(\frac{1+\gamma e^{-\kappa z}}{1-\gamma e^{-\kappa z}}\right), \tag{11}$$

where γ is an integration constant whose value is determined by equation 7:

$$\gamma = \frac{\sqrt{1+(y/2)^2}-1}{y/2}, \tag{12}$$

where

$$y = 4\pi\frac{\lambda_B\sigma}{\kappa}. \tag{13}$$

Inserting this into equation 3 gives us the ion concentrations

$$\rho_\pm(z) = \rho_s\left(\frac{1\mp\gamma e^{-\kappa z}}{1\pm\gamma e^{-\kappa z}}\right)^2. \tag{14}$$

The constants κ and λ_B have an important physical interpretation. We can see from its definition in equation 2 that the Bjerrum length is the distance at which the energy due to the Coulomb interaction of two particles with charge $\pm e$ is equal to its thermal energy k_BT. In water for instance, this is equal to 0.7nm. [7]. The Debye length is a property of the solvent and determines over what distance the ionic charge buildup near the wall decays as we can see from equation 14. In this these thesis we will only consider systems with a bulk concentrations of $\rho_s = 1$mM which corresponds to a Debye length of $\kappa^{-1} \approx 9.6$ nm.

Cylindrical geometry We have now solved the electrostatic equations in this simple case of an electrolyte near a single charged plane, but we are actually interested in the electrostatics of a nanopore. In cylindrical coordinates, the Poisson-Boltzmann equation takes the form

$$\frac{1}{r}\frac{d}{dr}\left(r\frac{\partial\phi}{\partial r}\right) = \kappa^2\sinh\phi(r), \tag{15}$$

where we once again assumed the system to be homogeneous in the $\hat{z}$ and $\hat{\theta}$ direction. This non-linear equation cannot be solved analytically however, so we need to make some approximations. For instance, for small values of ϕ we can approximate the Boltzmann distribution: [7]

$$\sinh(\phi) \approx \phi, \text{ if } |\phi| \ll 1. \tag{16}$$

Technically this would only be true for potentials $\psi < 25$mV at room temperature though in most applications it remains reasonably accurate up to 50mV. [10] For our purposes this approximation can therefore safely be made. Our linearised Poisson-Boltzmann equations can then be written as

$$\frac{1}{r}\frac{d}{dr}\left(r\frac{\partial\phi}{\partial r}\right) = \kappa^2\phi. \tag{17}$$

This equation can be solved in terms of special functions called *zero order modified Bessel functions of the first kind*, denoted as $I_0(r)$. [11] The solution where the potential is finite at $r = 0$ is given by

$$\phi(r) = BI_0(\kappa r), \tag{18}$$

where B is an integration constant to be determined by the boundary conditions. We require that $\partial\phi/\partial r = 4\pi\lambda_B\sigma$ at $r = R$, where R is the radius of our cylinder, similarly to what we did before, following the convention of Ref. [7] as opposed to Refs. [9–11] who require a fixed surface potential ψ_0 instead of a fixed surface charge σ. The derivative of this zero order Bessel function is simply the first order function [12, Eq. 10.29.3] so the potential will be given by

$$\phi(r) = 4\pi\lambda_B\sigma\frac{I_0(\kappa r)}{\kappa I_1(\kappa R)}. \tag{19}$$

However, instead of making an approximation for small ϕ we can also say that the channel is so large that the walls seem to be planar on the scale of Debye length, *i.e.* $R \gg \kappa^{-1}$. Then we can say that [13, Eq. B.1]

$$\frac{1}{r}\frac{d}{dr}\left(r\frac{\partial\phi}{\partial r}\right) \approx \frac{\partial^2\phi}{\partial s^2}, \tag{20}$$

where we defined a new coordinate $s = R - r$. This approximation would then yield the same Poisson equation 2 that we had for the planar wall but then as a function of coordinate s. We then get

$$\phi(s) = 2\log\left(\frac{1+\gamma e^{\kappa s}}{1-\gamma e^{\kappa s}}\right). \tag{21}$$

Both approximations are shown in figure 2 for four specific combinations of radii and surface charges, that are shown in four different colors. For each of those cases, there are two approximations, shown by dashed or solid lines. It should be noted that the $R \gg \lambda_D$ approximation is independent of R, so they are plotted on top of each other, hiding two lines. We see that the best approximation to use is dependent on the specific conditions and geometry of our system, since there are significant differences between the solutions. Later we will compare these to numerical results, to find out which one yields more accurate results.

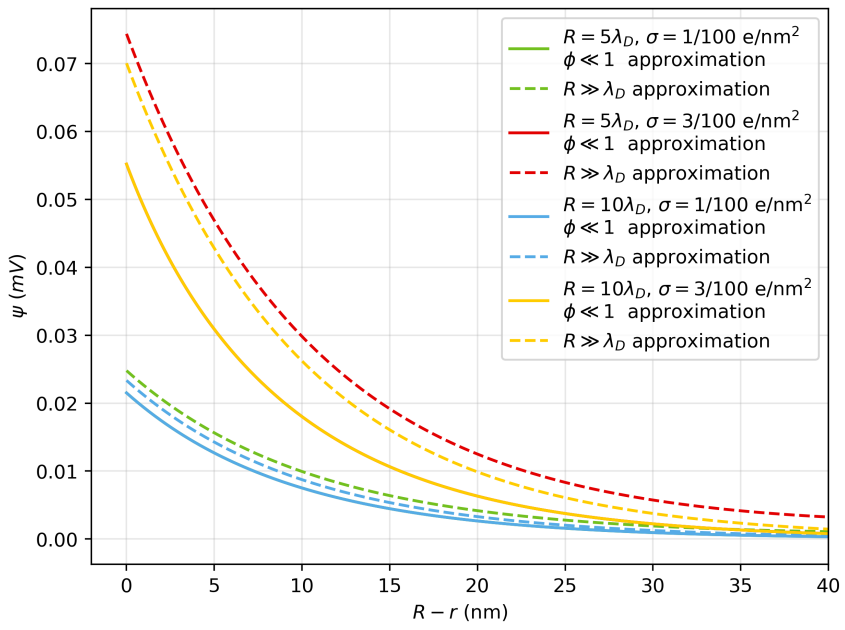

Figure 2: Potential in a cylindrical channel with various radii and surface charge densities. Both the large R approximation $R\kappa \gg 1$ of Eq 21 and the small ϕ approximation $\phi \ll 1$ of Eq 19 are shown.

3 Transport and Linear Response

The behavior of ions in a channel is not just dependent on the electrostatics as derived in the previous section. There we used the Poisson-Boltzmann equation to derive the charge distribution in equilibrium, but we are mostly interested in the response of our system to several driving forces. For instance, what happens when a pressure, chemical potential or electrical potential gradient is set up over the channel? As mentioned before, the most obvious answers would be that a pressure gradient induces a fluid flow, an electrical potential gradient causes a current, and a chemical potential gradient results in an ion flux. In our system, however, there are additional consequences of such a gradient due to the presence of the electrical double layer. Fluid flow, for instance, will now also transport some of the charge through the channel, causing an electrical current. Here we will consider the effects of a local pressure gradient $\partial_z p$ and a electrical potential gradient $\partial_z \psi$. For low driving forces, we can describe the flux associated with a a specific gradient with the Onsager matrix L [7] [13], in some literature also called the electrokinetic coupling matrix [14]:

$$\begin{pmatrix} Q \\ I \end{pmatrix} = A\mathbf{L} \begin{pmatrix} -\partial_z p \\ -\partial_z \psi \end{pmatrix}. \tag{22}$$

Here Q (m^3/s) is the fluid volume flux through the channel, I is the charge flux or current in Ampère and $A = \pi R^2$ is the cross section area of the channel. The Onsager matrix is symmetric *i.e.* $L_{12} = L_{21}$. This was proven by Lars Onsager in 1930 for systems close to equilibrium [15] and will not be shown here. Fortunately this reduces the number of matrix elements we need to compute. To derive these elements we need a set of equations to describe our full system which contains fluid flow, electrostatics and ionic fluxes.

3.1 Fluid Dynamics

Fluid flow can in our case be described by the Navier-Stokes equation for incompressible fluids. In our case this would be given by

$$\rho_m \frac{\partial \mathbf{u}}{\partial t} + \rho_m(\mathbf{u} \cdot \nabla)\mathbf{u} = -\nabla p + \eta(\nabla^2)\mathbf{u} + \mathbf{f}, \tag{23}$$

$$\nabla \cdot \mathbf{u} = 0, \tag{24}$$

where ρ_m is the mass density, $\mathbf{u}$ the fluid velocity, p the pressure, η the viscosity and $\mathbf{f}$ is a body force on the fluid. We only take an electric body force into account, caused by the interaction between ionic charge in the fluid with the electrical potential: $\mathbf{f} = -e\rho_e \nabla\psi$, where $\rho_e = \rho_+ - \rho_-$. In our case we are allowed to neglect several terms in the Navier-Stokes equation. This can be shown by looking at its dimensionless form [14]; we scale our variables as follows:

$$x_i^* = x_i/\ell, \tag{25}$$

$$\nabla^* = \frac{\nabla}{1/\ell}, \tag{26}$$

$$\mathbf{u}^* = \mathbf{u}/U, \tag{27}$$

$$p^* = \frac{p}{\eta U/\ell}, \tag{28}$$

$$\mathbf{f}^* = \frac{\mathbf{f}}{\ell^2/(\eta U)} \tag{29}$$

and

$$t^* = \frac{t}{U/\ell}. \tag{30}$$

Here we used a typical velocity U of our system, a typical length scale ℓ and consequently time scale U/ℓ and force $\ell^2/(\eta U)$. We then introduce the Reynolds number $\mathrm{Re} = \rho_m U\ell/\eta$ to write the dimensionless Navier-Stokes equation:

$$\mathrm{Re}\left(\frac{\partial \mathbf{u}^*}{\partial t^*} + (\mathbf{u}^* \cdot \nabla^*)\mathbf{u}^*\right) = -\nabla^* p^* + \nabla^{*2}\mathbf{u}^* + \mathbf{f}^*. \tag{31}$$

In our case we are looking at length scales of $\ell \sim 10^{-6}$ m, typical velocities in the range $U \sim 10^{-1}$ to 10^{-4} m/s, a viscosity $\eta \sim 10^{-3}$ Pa $\cdot$ s and $\rho_m \sim 10^3$ kg/m^3. We then find a Reynolds number somewhere in the 10^{-1} to 10^{-4} range. We can then conclude that in most cases we should be able to say that $Re \ll 1$ and that we can, therefore, neglect the terms on the left-hand side of equation 31. The Navier-Stokes equation then reduces to the Stokes equation:

$$\eta(\nabla^2)\mathbf{u} - \nabla p - e\rho_e \nabla\psi = 0. \tag{32}$$

It should be noted that ∇^2 denotes the vector Laplacian, which in Cartesian coordinates simply acts as $\nabla^2\mathbf{u} = (\nabla^2 u_x, \nabla^2 u_y, \nabla^2 u_z)^T$, but has a more complex form in spherical coordinates.

3.2 Ion Transport

The behavior of ions can be described with an extended Nernst-Planck equation for the ion fluxes. Barring any chemical reactions or miraculous cold nuclear fusion, the flux and ion density are related via [7] [3]

$$\frac{\partial \rho_\pm}{\partial t} = -\nabla \cdot \mathbf{J}_\pm. \tag{33}$$

For an ion species with valency ± 1, the flux is given by

$$\mathbf{J}_\pm = -D\left(\nabla\rho_\pm \pm \frac{e\rho_\pm}{k_B T}\nabla\psi\right) + \rho_\pm \mathbf{u}, \tag{34}$$

where we can distinguish multiple different contributions to this flux. First we have the diffusive flux that is proportional to the gradient of the ion species, $-D\nabla\rho_\pm$, where D is a diffusion constant. This constant does not necessarily need to be the same for all ions, but we will assume it here for the sake of simplicity. The second term is a conduction term, where an ion flux is induced by an applied electrical field. The third term is a convective one, where we take into account that the ions will be dragged along by any existent fluid flow.

3.3 Onsager Elements in a Cylinder

Equations 4, 32 and 34 now form a complete set of equations to describe our system, known as the PNPS-equations, short for Poisson, Nernst-Planck, Stokes. With these equations it is possible to derive analytical expressions for the Onsager matrix elements in a straight cylindrical channel [16] [6]. In this section we will use the approach of Werkhoven [6]. We consider the channel to be connected to two large reservoirs such that currents. Ions and water are allowed to enter or exit the reservoirs such that ion fluxes and mass fluxes through the channel are allowed. The ion concentrations are set to their bulk values at the far ends of the reservoirs. The Stokes equation is linear so the total flow profile is a sum of the pressure-induced and electro-osmotic flow, so we can treat them separately. In a long cylinder we can neglect any components of the fluid velocity and pressure gradient that are not in the z-direction, and u_z only depends on the radial coordinate so the Stokes equation reduces to

$$\frac{\eta}{r}\frac{\partial}{\partial r}\left(r\frac{\partial u_z}{\partial r}\right) = \partial_z p. \tag{35}$$

Note that here $\partial_z = -\Delta p/\ell$, which is a constant. We can solve this differential equation and find

$$u_z(r) = -\frac{\partial_z p}{4\eta} r^2 + C. \tag{36}$$

Requiring a so called no-slip condition where the fluid velocity has to be zero at the boundary $r = R$, where R is the radius of the cylinder, then yields the full flow profile

$$u_z(r) = -\frac{\partial_z p}{4\eta}(R^2 - r^2), \tag{37}$$

which is called Poiseuille flow. The local volumetric flow rate Q (in m/s) can then be found by integrating over the channel and dividing by the cross section area

$$Q = \frac{1}{\pi R^2}\int_0^{2\pi} d\theta \int_0^R r u_z(r) dr = \frac{R^2}{8\eta}\partial_z p, \tag{38}$$

so the first matrix element is given by

$$L_{11} = \frac{R^2}{8\eta}. \tag{39}$$

To find L_{12} for the streaming current it is best to transform to coordinate $s = R - r$ since we are only interested in the electrical double layer that's located close to the wall and we assume that the channel is much bigger than the Debye length $R \gg \lambda_B$. Then the current is given by

$$I = e\int_0^{2\pi} d\theta \int_0^R r\rho_e(r)u_z(r)dr \approx 2\pi eR\int_0^R ds u_z(s)\rho_e(s). \tag{40}$$

We can write this in terms of the non-dimensionalized potential with the Poisson-Boltzmann equation

$$I = 2\pi eR\left(-\frac{\varepsilon_0\varepsilon_r}{e^2\beta}\right)\int_0^R ds(\partial_s^2\phi)u_z(s). \tag{41}$$

This can be solved by using partial equation twice:

$$I = -2\pi eR\frac{1}{4\pi\lambda_B}\left(u_z\partial_s\phi|_0^R - \phi\partial_s u_z|_0^R + \int_0^R ds\phi\partial_s u_z\right). \tag{42}$$

Using $u_z(s=0) = \partial_s\phi(s=R) = \phi(s=R) = 0$ and $\phi(0) = \phi_0$ together with the first and second derivatives of u_z which can easily be obtained from equation 37, we find

$$\begin{aligned} I &= (-\pi R^2\partial_z p)\frac{1}{\eta}\left(\frac{e^2\beta}{4\pi\lambda_B}\psi_0 - \frac{2e}{4\pi\lambda_B R}\int_0^R \phi ds\right) \\ &= (-\pi R^2\partial_z p)\frac{1}{\eta}\left(\varepsilon_0\varepsilon_r\psi_0 + \frac{e\lambda_D}{2\pi R\lambda_B}P_1\right). \end{aligned} \tag{43}$$

Where P_1 is defined as

$$P_1 = \frac{-1}{\lambda_D}\int_0^R ds\phi(s). \tag{44}$$

This integral can be solved exactly in terms of so-called polylogarithmic functions if we take the large-radius approximation to find ψ in equation 21, according to Werkhoven [6], but we can also easily solve the integrals numerically, since we have an analytical expression for ϕ. We can now divide I by $(-\pi R^2\partial_z p)$ to find L_{12}:

$$L_{12} = \frac{1}{\eta}\left(\varepsilon_0\varepsilon_r\psi_0 - \frac{e\lambda_D}{2\pi R\lambda_B}P_1\right). \tag{45}$$

Which is in agreement with Werkhoven [6]. The last Onsager matrix element is given by the current that is induced by an applied electric field. We have two contributions to this; the advective component due to the electro-osmotic flow and a conductive term. The conductive term of the current can be found by integrating the conductive terms of the Nernst-Planck equation:

$$\begin{aligned} I_{cond} &= 2\pi e\int_0^R r dr(j_{+,z}^{cond} - j_{-,z}^{cond}) \\ &= 2\pi\beta De^2 E\int_0^R r dr(\rho_+ + \rho_-) \\ &= 4\pi\beta De^2 E\rho_s\int_0^R dr r(\cosh(\phi)). \end{aligned} \tag{46}$$

Where we once again assumed that the two ion species have the same diffusion coefficient, and used the Boltzmann equation. The cosh of ϕ, however is not only non-zero in the EDL so we cannot immediately switch to coordinate $s = R - r$. To do this we split the integral in two:

$$\begin{aligned} I_{cond} &= 4\pi\beta De^2 E\rho_s \left(\int_0^R r dr + R \int_0^R ds(\cosh[\phi] - 1) \right) \\ &= 4\pi\beta De^2 E\rho_s \left(\frac{1}{2}R^2 + R\lambda_D P_2 \right) \\ &= (\pi R^2 E) D\varepsilon_0\varepsilon_r \frac{1}{\lambda_D^2}(1 + \frac{2\lambda_D}{R}P_2). \end{aligned} \tag{47}$$

Where P_2 is defined as

$$P_2 \equiv \frac{1}{\lambda_D}\int_0^R ds(\cosh[\phi] - 1). \tag{48}$$

For the advective term we need to find an expression for the electro-osmotic flow for $\partial_z p = 0$. The Stokes equation is then given by:

$$\eta\nabla^2 u - \rho_e \nabla\psi = 0. \tag{49}$$

And, using the Poisson equation and integrating twice, we find

$$u_z(s) = -\frac{\varepsilon_0\varepsilon_r\nabla\psi}{\eta}(\psi(s) - \psi_0). \tag{50}$$

The current is the given by the integral over this electro-osmotic flow times the ionic charge

$$I_{adv} = 2\pi eR\int_0^R ds\frac{\varepsilon_0\varepsilon_r E}{\eta}(\psi(s) - \psi_0)\rho_e(s). \tag{51}$$

We know that $\rho_e = -\frac{\varepsilon_0\varepsilon_r}{e^2\beta}\partial_s^2\phi$ and $\psi = \phi/(e\beta)$ so we can write this integral as

$$I_{adv} = -2\pi R\left(\frac{\varepsilon_0\varepsilon_r}{e\beta}\right)^2 \frac{E}{\eta}\int_0^R ds(\phi(s) - \phi_0)\partial_s^2\phi. \tag{52}$$

We can split this into two integrals, such that

$$I_{adv} = -2\pi R\left(\frac{\varepsilon_0\varepsilon_r}{e\beta}\right)^2 \frac{E}{\eta}(z_1 - z_2), \tag{53}$$

where we defined

$$z_1 \equiv \int_0^R ds\phi(s)\partial_s^2\phi(s), \tag{54}$$

$$z_2 \equiv \int_0^R ds\phi_0\partial_s^2\phi(s). \tag{55}$$

We can begin solving z_1 by performing integration by parts

$$z_1 = (\phi\partial_s\phi)|_0^R - \int_0^R ds(\partial_s\phi)^2. \tag{56}$$

To solve this last integral we can perform a trick to find an expression for $(\partial_s\phi)^2$. [17] We start with the Poisson-Boltzmann equation and multiply both sides with $(\partial_s\phi)$ such that we get

$$(\partial_s\phi)(\partial_s^2\phi) = \kappa^2(\partial_s\phi)\sinh(\phi). \tag{57}$$

Now we can recognize that both sides are actually the derivatives with respect to s of $\frac{1}{2}(\partial_s\phi)^2$ and $\kappa^2\cosh(\phi)$ respectively. We can integrate this to find

$$\frac{1}{2}(\partial_s\phi)^2 = \kappa^2(\cosh(\phi) + c), \tag{58}$$

where c is an integration constant. Now, we know that the potential is only non-zero near the EDL, so far from the wall $\cosh(\phi) + c \to 0$ for $\phi \to 0$. This suggests that $c = -1$ since $\cosh(0) = 1$, provided $R \gg \lambda_D$. The integral z_1 can then be written as:

$$\begin{aligned} z_1 &= 4\pi\lambda_B\sigma\phi_0 - 2\kappa^2 \int_0^R ds(\cosh[\phi] - 1) \\ &= 4\pi\lambda_B\sigma\phi_0 - \frac{2}{\lambda_D}P_2, \end{aligned} \tag{59}$$

where we used that $\phi(s = R) = 0$, $\phi(0) = \phi_0$, $\partial_s\phi(0) = -4\pi\lambda_B\sigma$ and $\kappa^2 = \lambda_D^{-2}$. The second integral z_2 is easier to solve since ϕ_0 does not depend on s. The solution becomes much clearer when we write it in terms of ρ_2 again:

$$z_2 = -\frac{e^2\beta}{\varepsilon_0\varepsilon_r}\phi_0 \int_0^R ds\rho_e(s). \tag{60}$$

But if we require our entire system to be electro-neutral then the integral over ρ_e must simply be $-\sigma$ since the surface charge must cancel the ionic charge in the fluid. This means that

$$z_2 = \frac{e^2\beta}{\varepsilon_0\varepsilon_r}\phi_0\sigma = 4\pi\lambda_B\sigma\phi_0. \tag{61}$$

Filling everything back into equation 53 we finally get

$$\begin{aligned} I_{adv} &= -2\pi R\frac{E}{\eta}\left(\frac{\varepsilon_0\varepsilon_r}{e\beta}\right)^2(4\pi\lambda_B\phi_0\sigma - \frac{2}{\lambda_D}P_2 - 4\pi\lambda_B\phi_0\sigma) \\ &= 4\pi R\frac{E}{\eta}\left(\frac{e}{4\pi\lambda_B}\right)^2\frac{1}{\lambda_D}P_2 \\ &= (\pi R^2 E)\frac{4}{\eta}\left(\frac{e}{4\pi\lambda_B}\right)^2\frac{1}{R\lambda_D}P_2. \end{aligned} \tag{62}$$

We now have all the terms we need to write down the last matrix element:

$$\begin{aligned} L_{22} &= \frac{I_{adv} + I_{cond}}{\pi R^2 E} \\ &= \frac{4}{\eta}\left(\frac{e}{4\pi\lambda_B}\right)^2\frac{1}{R\lambda_D}P_2 + \frac{\varepsilon_0\varepsilon_r D}{\lambda_D^2}(1 + \frac{2\lambda_D}{R}P_2). \end{aligned} \tag{63}$$

This is in agreement with Werkhoven [6].

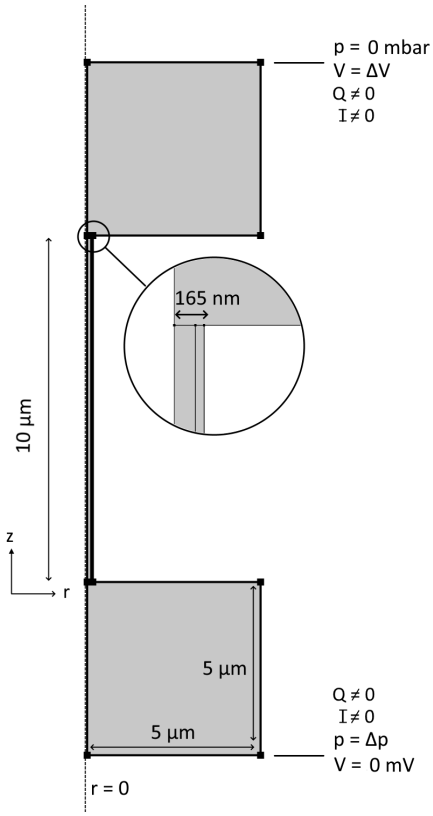

Figure 3: Illustration of the COMSOL geometry. The rotation axis is shown with the dotted line, situated at $r = 0$.

4 Numerical Results in a Cylindrical Geometry

We now want to solve the governing PNPS equations numerically in a cylindrical geometry for which we will use finite-elements software called COMSOL MULTIPHYSICS. We take a cylinder of length $\ell = 10\mu$m and radius of 165 nm that is connected on both ends with a large reservoir that contain a bulk electrolyte with a concentration of $2\rho_s \equiv \rho_{s-} + \rho_{s+} = 2$ mol/m^3. To this channel we can apply a pressure gradient or electrical field and the wall of the cylinder has a surface charge of $e\sigma = +0.0032044$ C/m^2, which is equivalent to two elementary charges per 100 nm^2. The situation is illustrated in figure 3. We allow ions and water to exit the reservoirs such that a current can be generated.

Electric Potential In section 2 we derived two different approximations for the electrical potential as a function of the radial coordinate. For convenience, we first take a solution where the applied electrical field is zero. The result is plotted in figure 5 along with the analytical solution to the linear PB-equation and the analytical expression for the potential near a planar wall. We see that the planar-wall solution is considerably better suited to describe the potential than the linearized approximation in a cylinder. The radius is in this much larger than the Debye length, and the potential at the wall exceeds the limit for linearization. The linearized solution might perform better for thinner channels or smaller surface charges.

Fluid Velocity When various pressure gradients and electric fields are applied to the system we see velocity fields as shown in figure 6. The theoretical expressions are shown in the solid lines, while the numerical values are dotted. We see that they match almost perfectly.

Linear Response In the previous section we derived how the electric current I is dependent on the applied pressure and electric field. These relationships were all linear in both Δp and ΔV with prefactors that were

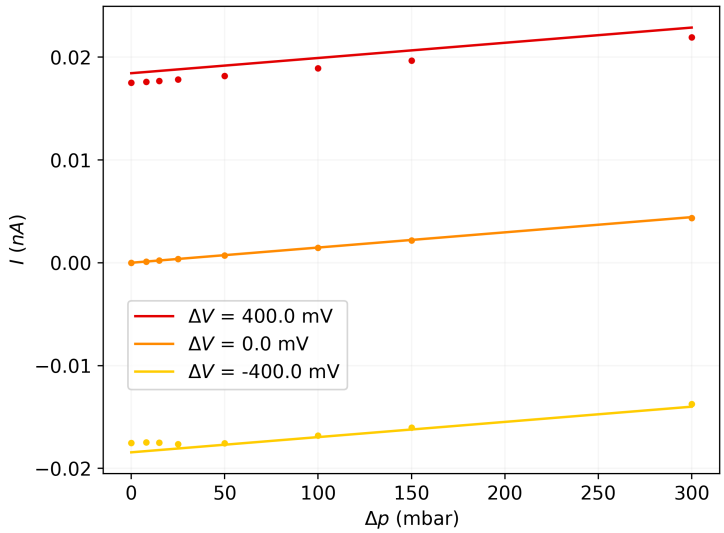

Figure 4: Ionic current as a function of the applied pressure. Both the theoretical predictions from equations 45 and 63 (solid) and the numerical values (dotted)

partly determined by two integrals that depended on the potential, that could be calculated analytically in terms of special functions, but were simply calculated in Mathematica here. The result was $P_1 = 1.50784$. and $P_2 = 0.638373$. The linear response expressions from equations 45 and 63 are shown in figure 4 together with the numerical values that were obtained by integrating over the fluxes in the channel in COMSOL. Overall, everything does seem to be in agreement with the theoretical predictions. A few things stand out; the first thing we notice is that the current response for $\Delta V = -400mV$ is not completely linear in Δp. The effect is very small compared to the total current and is likely due to a numerical error. We also see that the theoretical prediction for $\Delta V = 400$ mV is off by a fixed amount, meaning that the channel exhibits a very small but noticeable diode-like effect in the numerical calculations.

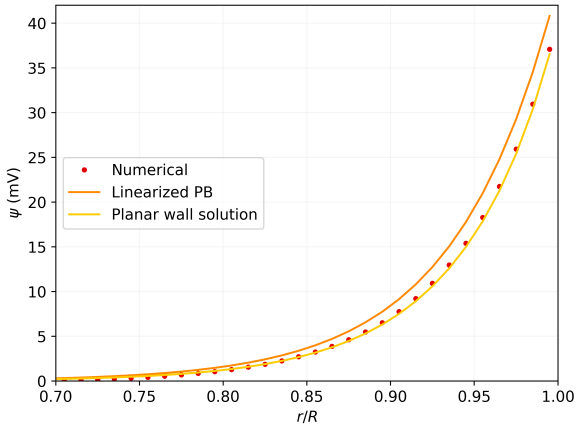

Figure 5: Electrical potential as a function of the radial coordinate, normalized by the channel radius R. The numerical solution is shown dots; the theoretical approximations from equations 21 and 19 are shown as solid lines

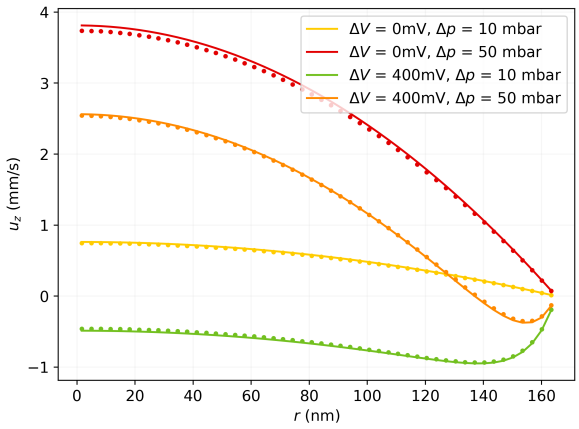

Figure 6: Velocity field as a function of the radial coordinate for different pressure and electrical potential gradients. Numerical solutions are dotted; the theoretical expressions are shown as lines

5 Numerical Solutions in Conical Geometries

We now want to model the conical geometry that was used in the experiment by Jubin *et al.* [8]. Like Jubin, we look at cones with an opening angle of $\alpha = 5°$. Building such a model does, however, require some care to be taken. When applying an electric field across the straight cylindrical channel, it is clear that the electric field lines will be parallel to the wall of the channel and to each other. In a cone, however, it is conceivable that some of the field lines 'leak' to the environment through the channel walls. If this is the case, then we cannot get away with building the channel inside a vacuum as we effectively did in the case of a cylinder, but we would need to model both the glass of the pipette and the environment around the pipette that forms the nanochannel in the experimental setup. It would, however, be very computationally heavy to perform the same range of simulations for different Δp and ΔV in this more complicated geometry. To test whether the naive geometry as shown in figure 7 is an acceptable approximation of the experimental setup, we built a system that closely resembles the experimental setup from Jubin *et al* [8], as shown in figure8. Glass has a relative permittivity of 5 - 10 [18], so we modeled glass with $\varepsilon_r = 5$ and a thickness of 80nm. Note that glass has a negative surface charge, so we take $e\sigma = -0.0032044$ C/m^2. We use the same boundary conditions we used in the previous section in the cylindrical geometry. The model yields the electrical potential and the electric field lines that are shown in 9. We can see that the electrical field does not seem to permeate the glass walls of the cone and that we are therefore allowed to use the simpler model as shown in figure 7, where we do not take the glass and the environment outside of the pipette into account.

We expect several quantities to exhibit heterogeneities in the nanopore, such as the space charge as predicted by Jubin *et al.* [8] The charge distributions for $\Delta V = 400$mV and $\Delta V = -400$mV are shown in figures 11 and 10. The EDL is visible as the red band around the wall. Note that we are now looking at charges of around 10^1C/m^3 whereas the EDL itself can be up to 10^5C/m^3. These charges seem relatively small in comparison to the EDL and it is questionable whether this would have any impact on the current. We see the strongest space charges at low pressure gradients, while they seem to vanish around the 50mbar. The sign of the charge is interesting since both cases have a negative charge around the tip for low pressure and positive charge for slightly higher pressures. The biggest difference seems to lie in the magnitude of the charge, though there are small differences; at $\Delta p = 0$ we see a small positive charge below the negative for $\Delta V = 400$mV, while it is not present in the case of $\Delta V = -400$mV.

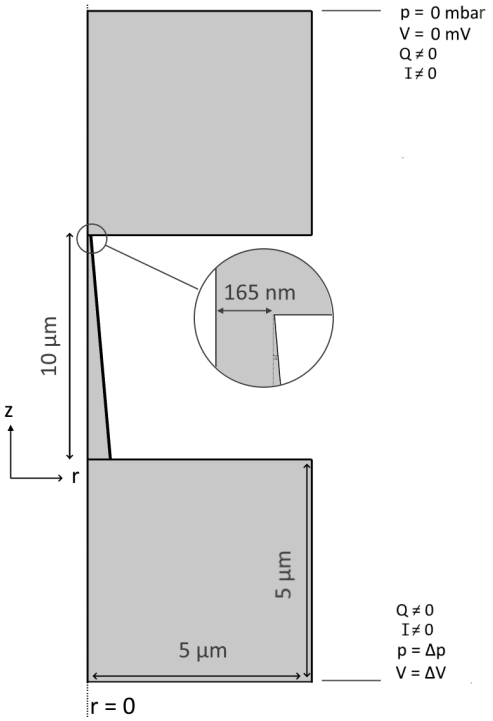

Figure 7: Illustration of a naive COMSOL geometry. The rotation axis is situated at $r = 0$.

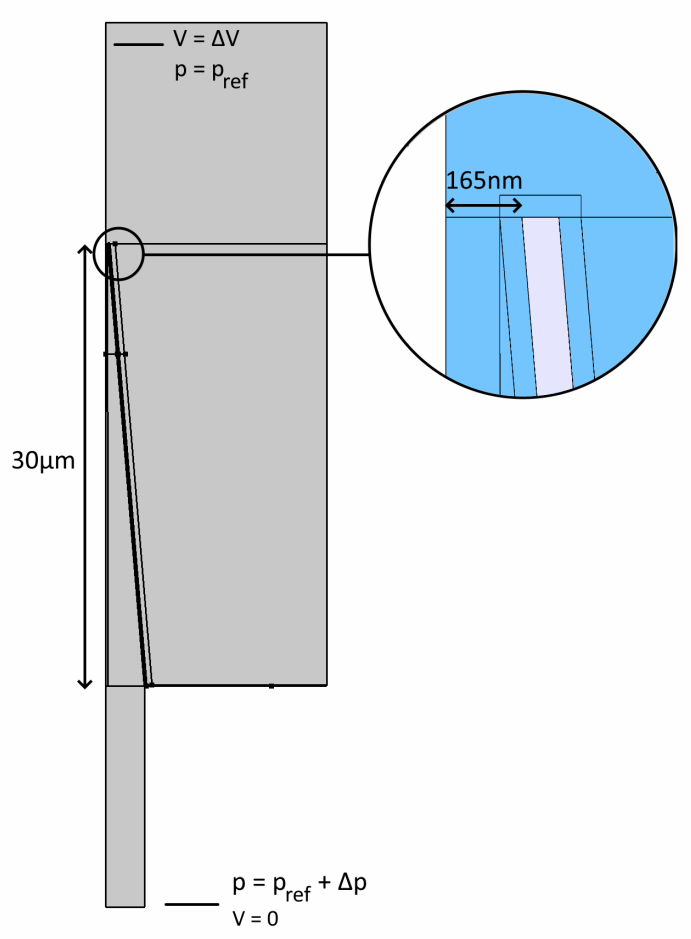

Figure 8: Illustration of a more involved COMSOL geometry. The rotation axis is situated at $r = 0$. The blue color in the insert represents water with the electrolyte and the grey represents the glass.

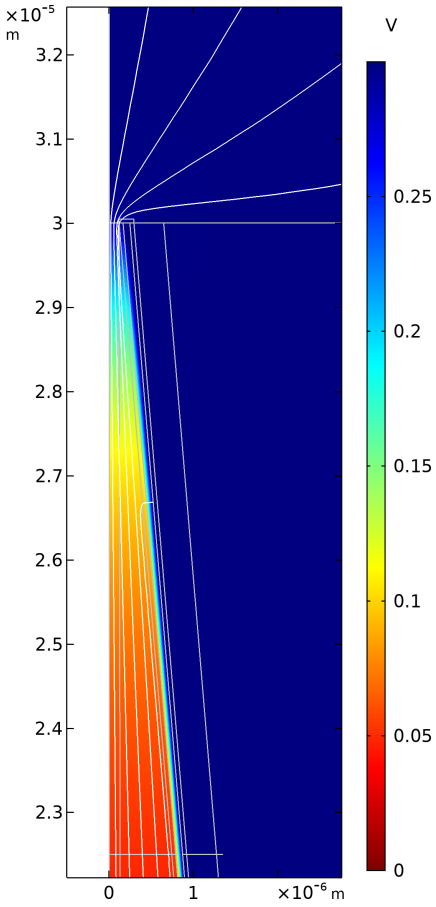

Figure 9: Electrical potential in the tip of the conical pipette and the field lines of the electric field (white). Lines of the geometry are shown in grey.

The pressure induced current I_p is defined as $I_p = I(\Delta V, \Delta p) - I(\Delta V, \Delta p = 0)$. The response of I_p is shown in figure 12 and we immediately see a big difference with the results from Jubin ET AL.. For negative ΔV there seems to be negative 'bump' the first few millibar of pressure. This means that for very small pressures, the total current becomes more negative instead of higher as we expected. The discrepancy between the numerical solution and the experimental data is unexpected and we will have to develop more theory to fully understand the situation. It is interesting to note that the fluid flow profile changes sign around the same pressure as the current goes from decreasing to increasing.

Besides the total current response, we can differentiate between different contributions of the fluxes with COMSOL, to find out which contributions to the total current cause the non-linearity. This is shown in figure 13, where we see the total pressure-induced current plotted with its different constituent currents. The non-linear behavior is clearly caused by the conductive current, which is surprising since the conductive current does not depend on the pressure in a cylindrical channel. As we saw in section 3, the conduction current is generated by the salt concentration $\rho_s \equiv \rho_+ + \rho_-$, so there must be a depletion or accumulation of ions in the channel that depends on the pressure. This is exactly what we see in figures 14 and 15. Here we see a non-homogeneous concentration profile through the channel which causes a non-homogeneous conductivity. The difference between the profiles is maybe even more interesting since we see that the difference between the concentration profiles behaves non-linearly when the pressure is increased in constant increments of 5mbar.

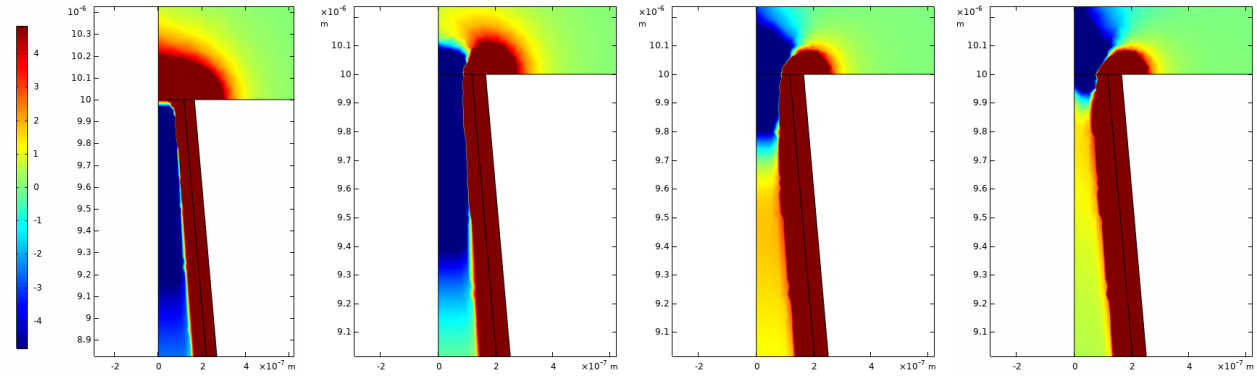

Figure 10: Space charge in $\mathrm{C/m^3}$ for $\Delta V = -400\mathrm{mV}$ and (from left to right) a pressure difference of 0, 8, 25 and 50mbar

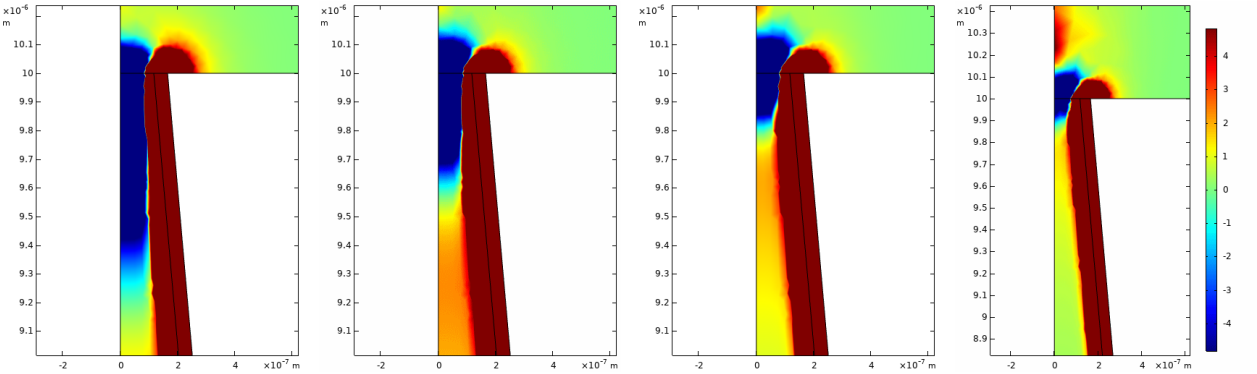

Figure 11: Space charge in $\mathrm{C/m^3}$ for $\Delta V = 400\mathrm{mV}$ and (from left to right) a pressure difference of 0, 8, 25 and 50mbar

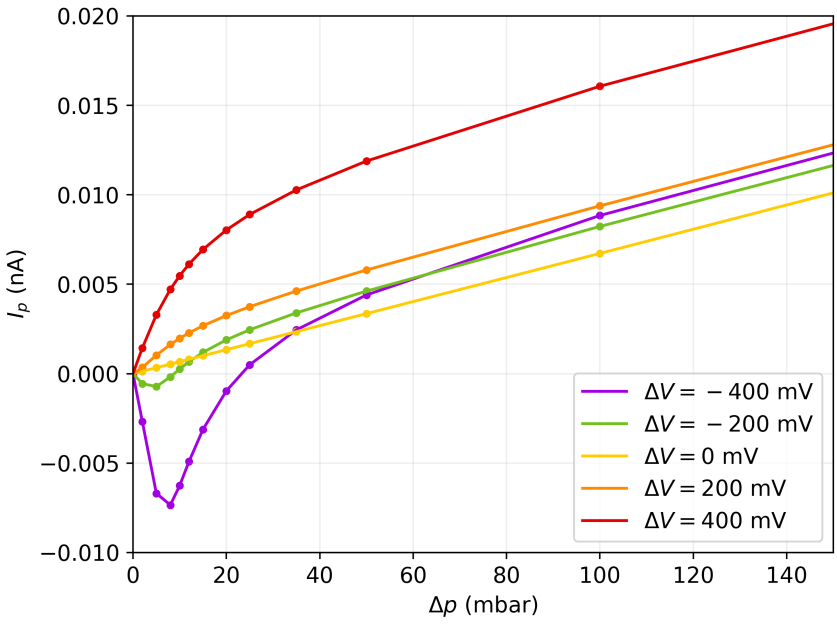

Figure 12: Pressure-induced current as a function of the pressure. Figure is zoomed in on the non-linear part.

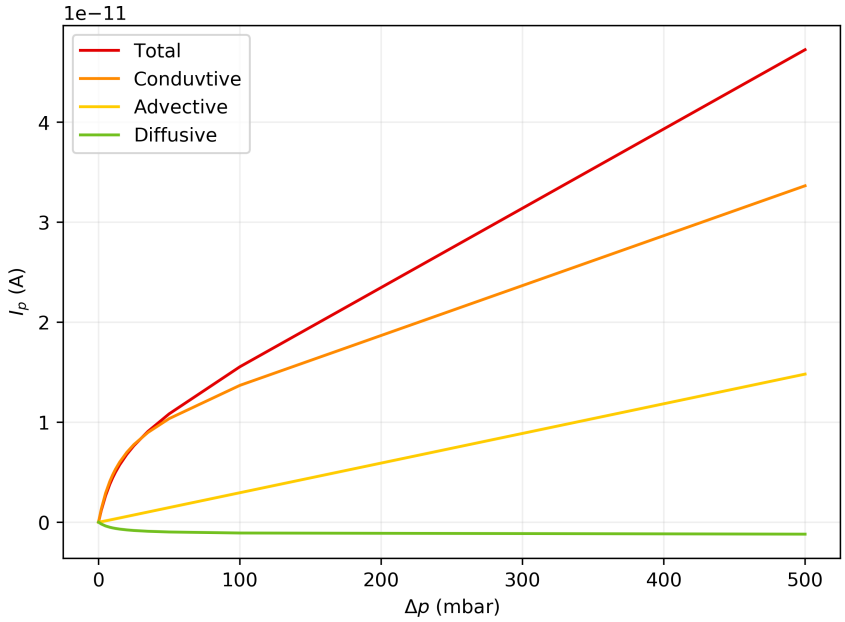

Figure 13: Different pressure-induced contributions to the current and the total pressure induced current as a function of Δp for $\Delta V = +400\text{mV}$

Comparing the simulations with $\alpha = 0°$ and $\alpha = 5°$ we see a few key differences. There is a space charge present in the cone that is not present in the cylinder. This space charge does seem to depend on the pressure, but it is unlikely that it influences the current in a significant manner. This is also suggested by the fact that the advection current in figure 13 is linear and that the non-linear behaviour seems to be entirely caused by the conductive current, which does not depend on charge. The conduction current in a cone is dependent on the pressure, whereas it is not in a cylinder. This seems to be caused by an homogeneity in the concentration profile in a cone that is absent in a cylinder. This concentration profile is influenced by the pressure in a non-linear fashion, which would induce a non-linear conductivity.

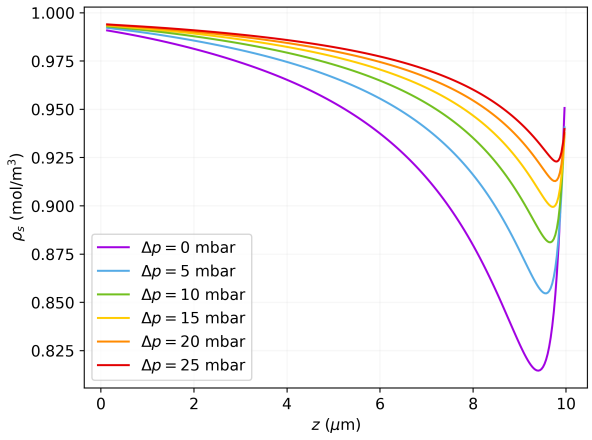

Figure 14: Concentration profile on the central axis for different pressures at $\Delta V = 400\text{mV}$

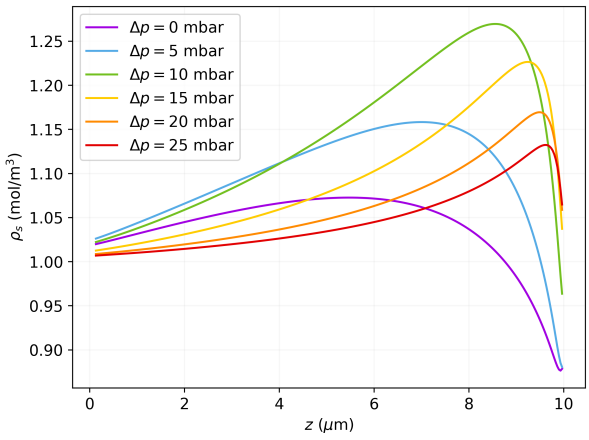

Figure 15: Concentration profile on the central axis for different pressures at $\Delta V = -400\text{m}$

6 Analytical Theory in a Conical Geometry

In sections 2 and 3 we discussed the electrokinetics in the simple case of a cylindrical nanopore, and the linear response relations that followed. Here our goal is to find a theoretical description to explain the phenomena that were described by section and Jubin *et al.*[8]. The depletion and accumulation of ions a in conical nanopore is a known phenomena in the literature [19] [20] [21] [22], since it also causes another phenomenon: current rectification. Current rectification is essentially a diode-like behavior of a channel. In conical channels, or other channels with symmetry breaking in geometry or surface charge, often exhibit an asymmetry in the $I-V$ curve, the current as a function of the applied electric field. This has to do with the fact that the tip of the cone has a higher area/volume ratio than the base. [20]. We will try to capture this phenomenon by deriving expressions for the different contributions to the salt flux and requiring them to be constant throughout the channel.

To find an analytical expression for the conduction current in conical geometry, we need to find expressions for the electric field, fluid velocity profile and salt concentration profiles.

6.1 Electric Field

We observed in section that no electric field lines seemed to escape the pipette, even when the environment around the cone was modeled. We can then say that the the applied electrical field, integrated over a slice of the cone, should be a constant throughout the nanopore. This means

$$\int_0^{2\pi} d\theta \int_0^{R(z)} dr r \bar{E}_z^{appl.} = \gamma, \tag{64}$$

where $\bar{E}_z^{appl}$ is the average applied electrical field in the z-direction, $R(z) = R_0 + az$, with $a = R_d/\ell = \tan\alpha$, is the radius of the cone at height z measured from the small opening of the cone and γ is some constant that is yet to be determined. The average electrical field is independent of r so we can solve this integral, and solve for $\bar{E}_z^{appl}$:

$$\bar{E}_z^{appl}(z) = \frac{\gamma}{\pi R(z)^2} = \frac{\gamma}{\pi(R_0 + az)^2}. \tag{65}$$

A value for γ can be found analytically, since we know that $E = -\nabla\psi$. We can integrate equation 65:

$$\psi(z) = -\int \frac{\gamma dz}{\pi(R_0 + az)^2} = \frac{\gamma}{a\pi(R_0 + az)} + c \tag{66}$$

Where c is an integration constant that is fixed by $\psi(0) = 0$, such that

$$c = -\frac{\gamma}{a\pi R_0} \tag{67}$$

Consequently from the condition that $\psi(\ell) = \Delta V$ we find

$$\gamma = -\frac{\Delta V}{\ell}\pi R_0(R_0 + R_d) \tag{68}$$

Inserting γ into equation 65, we find

$$\psi^{appl}(z) = \Delta V R_0 \left(1 + \frac{R_0}{R_d}\right)\left(\frac{1}{R_0} - \frac{1}{R_0 + az}\right), \tag{69}$$

which can be rewritten to the form

$$\psi^{appl}(z) = \frac{\Delta V}{\ell}\frac{(R_0 + R_d)}{R_0 + az}z. \tag{70}$$

6.2 Fluid Flow

We consider a cone of length ℓ, opening angle α and a radius between R_0 at the tip and R_d at the bottom, as shown in Figure 16. We take the origin of a spherical coordinate system $(r,\, \theta)$ at O, the (virtual) vertex of the cone. In reality this point would be located somewhere in our reservoir, but it allows us to describe the converging or diverging flow in terms of streamlines of constant angle θ. The flow profile for a full cone with a point source in its vertex is given by [23]:

$$u_r = \frac{3q}{2\pi r^2} \frac{\zeta^2 - \zeta_0^2}{(1+2\zeta_0)(1-\zeta_0)^2} \tag{71}$$

with a pressure given by [24]:

$$p = p_\infty - \frac{\eta q}{\pi r^3} \frac{1-3\zeta^2}{(1+2\zeta_0)(1-\zeta_0)^2} \tag{72}$$

With $\zeta = \cos\theta$ and $\zeta_0 = \cos\alpha$, and where p_∞ is the pressure at infinity, η the viscosity, and q is the volumetric flow rate through the channel. It should be stressed that the $\hat{r}$ direction is not the radial coordinate in cylindrical coordinates here, but the spherical coordinate, pointing away from the origin O. For small angles α, we can make the approximation that $\cos\theta \approx 1 - \frac{1}{2}\theta^2$, such that equation 71 reduces to

$$u_r \approx \frac{2q}{\pi r^2 \alpha^4}[(\alpha^2 - \theta^2)] \tag{73}$$

and

$$p = p_\infty - \frac{8\eta q}{3\pi\alpha^4 r^3} \tag{74}$$

Going back to our cylindrical coordinates, taking the origin of our coordinate system back to the bottom of the cone and using that $\cos\alpha \approx 1$ such that $r \to z_0 + \ell - z$, we find

$$u_z \approx \frac{2q}{\pi\alpha^4(\ell + z_0 - z)^2}\left(\alpha^2 - \arctan\left(\frac{r}{\ell + z_0 - z}\right)\right) \tag{75}$$

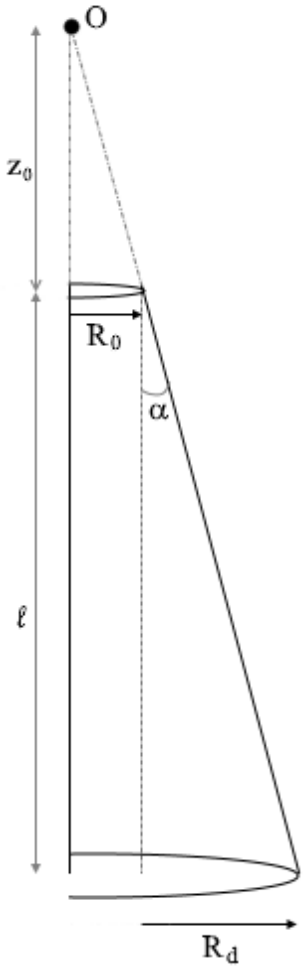

Figure 16: Half the geometry of the nanopore, with the origin in the vertex of the cone.

All these expression are in terms of the volumetric flow rate q, but by imposing the right boundary conditions on equation 74, we can find an expression for q as a function of Δp. We impose $p(0) = p_{in}$ and $p(\ell) = p_{in} + \Delta p$. This yields

$$-\frac{8\eta q}{3 * \pi * \alpha^4} \frac{1}{(\ell + z_0)^3} = \Delta p - \frac{8\eta q}{3\pi\alpha^4} \frac{1}{z_0^3} \tag{76}$$

which can be rewritten as

$$q = \frac{3\pi\alpha^4}{8\eta} \frac{z_0^3(\ell + z_0)^3}{(\ell + z_0)^3 - z_0^3} \Delta p \tag{77}$$

The derivative of the pressure can then be written as

$$\partial_z p(z) = \frac{3\Delta p}{(\ell + z_0 - z)^4} \frac{z_0^3(\ell + z_0)^3}{(\ell + z_0)^3 - z_0^3}, \tag{78}$$

And in the low angle approximation, we find that equation 73 reduces to a Poiseuille flow:

$$u_z(r) = -\frac{\partial_z p}{4\eta}(R(z)^2 - r^2) = -\frac{1}{4\eta} \frac{3\Delta p}{(\ell + z_0 - z)^4} \frac{z_0^3(\ell + z_0)^3}{(\ell + z_0)^3 - z_0^3}(R(z)^2 - r^2) \tag{79}$$

This derivation does not take any charge density or electric field into account and the flow profile and expressions for the volumetric flow rate and pressure will therefore deviate from the numerical values. The

pressure near the wall of the cone, will be higher due to body force that is generated by the attraction between the surface charge and the electric double layer. For the most part, however, we see a Poiseuille-like flow profile for low cone opening angles, where the natural coordinates are the angle and distance from the origin, since the flow in the $\hat{\theta}$ direction is zero. The applied electric field will also heavily contribute to the flow profile in the form of an electro-osmotic flow profile, so we need to extend the argument to account for this. The general expression for electrically driven fluid flow could not be found analytically but for small angles we can guess that a plug-flow will be a good approximation. In section 3 we derived that in a cylinder the flow profile is given by:

$$u_z(r,z) = -\frac{\varepsilon_0\varepsilon_r\partial_z\psi_{appl}}{\eta}(\psi_s - \psi(s)) \tag{80}$$

The surface potential of the wall at a certain height z is, however, not necessarily the correct surface potential to use in this expression since the wall makes an angle with the central axis. For a point at height z, the closest point on the wall is Δz higher where $\Delta z = (R(z) - r)\sin\alpha\cos\alpha$. For small angles α, however, $\sin\alpha\cos\alpha$ is negligible, suggesting that the plug flow as given in equation 80 could be a reasonable approximation. It is, however, not a solution of the Stokes equations, as the volumetric flow rate through the channel is not generally a constant throughout the channel with this expression[25], which is not allowed in an incompressible fluid. This causes additional pressure gradients, even when no pressure difference is applied. An expression for this pressure gradient could be found by calculating a z-dependent volumetric flow rate $Q(z)$ by integrating equation 80 and the difference between $Q(z)$ and $Q(\ell)$ at the wide end, and equating that to the volumetric flow rate of a Poiseuille flow. In qualitative terms, velocity must increase or decrease when the radius of the channel decreases or increases, respectively, in the direction of the flow. This is however not generally proportional to the driving force. A pressure gradient must be created to compensate for the discrepancy between the two. This effect is of second order however, and for simplicity we will assume that the additional pressure gradients are negligible.

6.3 Salt Transport

Since we need the concentration profile to calculate the conduction current, we are going to try to find an expression for the total flux through the channel, which must be constant throughout the channel. We can then solve for the concentration profile. As we saw before, ion transport is governed by the Nernst-Planck equation:

$$j_\pm = -D\nabla\rho_\pm \pm e\beta D\rho_\pm\nabla\psi + u\rho_\pm. \tag{81}$$

The total excess salt transport given by $j_{tot} = j_+ + j_- - 2u\rho_b$, where ρ_b is the bulk concentration in the reservoirs, is given by

$$j_{tot} = -D\nabla\rho_s + e\beta D\rho_e\nabla\psi + u(\rho_s - 2\rho_b), \tag{82}$$

where we defined $\rho_s(r,z) = \rho_+ + \rho_-$, and $\rho_e = \rho_+ - \rho_-$ and from section 2 we know that $\rho_s(r,z) = 2\bar{\rho}_s(z)\cosh(\phi)$ with $\bar{\rho}_s$ is the salt concentration along the rotation axis of the channel. We now want to radially integrate the z-component of expression to find the total salt flux J_{tot}. We can split it up into three integrals:

$$J_{tot} = 2\pi\int_0^{R(z)} r j_{tot}dr = J_{dif} + J_{cond} + J_{adv}, \tag{83}$$

where

$$J_{dif} = -2\pi D\int_0^R r\partial_z\rho_s(r,z)dr, \tag{84}$$

$$J_{cond} = 2e\pi\beta D\int_0^R r\rho_e(r,z)\partial_z\psi(r,z)dr, \tag{85}$$

and

$$J_{adv} = 2\pi\int_0^R r u_z(r,z)(\rho_s(r,z) - 2\rho_b). \tag{86}$$

Starting with the diffusion flux J_{dif}, we can make the approximation that $\partial_z \rho_s(r,z) \approx 2\cosh[\phi(r)]\partial_z \bar{\rho}_s$. Here we ignore the z-derivative of ψ that is generated by the fact that the EDL is not parallel to the z-axis, because this should be canceled out in equilibrium by a term in J_{cond}, which we will also ignore. The integral of equation 84 can be written as

$$\begin{aligned} J_{dif} &= -4\pi D \partial_z \bar{\rho}_s \int_0^R r\cosh(\phi) dr \\ &= -4\pi D \partial_z \bar{\rho}_s \left(\frac{1}{2} R(z)^2 + R(z)\bar{\lambda}_D P_2 \right). \end{aligned} \tag{87}$$

Here $\bar{\lambda}_D$ is the Debye length that is calculated with the bulk ion concentration, instead of the local concentration. In other words, we neglect the deformation of the EDL due to a varying concentration profile $\bar{\rho}_s$. P_2 is the PB integral as defined by Werkhoven [6]:

$$P_2 = \frac{1}{\bar{\lambda}_D} \int_0^R ds(\cosh(\phi) - 1), \tag{88}$$

which is a dimensionless constant. For the conduction integral J_{cond} we split the charge ρ_e into a Poisson-Boltzmann charge $\rho_e^{pb}(r,z)$ of the EDL and an extra contribution of a space-charge $\rho_e^{sp}(z)$. We also split the potential $\psi(r,z)$ into a potential $\psi_{appl}(z)$ due to the applied electric field and a Poisson-Boltzmann potential $\psi(r,z)$ of which we will ignore the z-derivative, as mentioned before. We get

$$\begin{aligned} J_{cond} &= 2e\pi\beta D \int_0^R r(\rho_e^{pb} + \rho_e^{sp}) \partial_z \psi_{appl}(z) dr \\ &= 2e\pi\beta D \partial_z \psi_{appl} \left(\frac{1}{2} \rho_e^{sp}(z) R(z)^2 + \sigma R(z) \right), \end{aligned} \tag{89}$$

where we recognized that

$$\int_0^R \rho_e^{pb} r dr = \sigma R(z). \tag{90}$$

The advection integral from equation 86 is given by

$$J_{adv} = 2\pi \int_0^R r(\rho_s - 2\rho_b)(u_{EO} + u_p) dr, \tag{91}$$

where we split the velocity profile u into a pressure induced flow u_p and an electro-osmotic flow u_{EO}. We do need to simplify the flow profiles in the cone, however. We will assume that locally $u(r,z)$ can be approximated by the $u(r,z)$ in a cylinder with radius $R(z)$, such that we can use a Poiseuille flow and a plug flow for the pressure-induced and electro-osmotic flow, respectively. They are given by

$$u_p(r,z) \approx -\frac{\partial_z p}{4\eta}(R(z)^2 - r^2), \tag{92}$$

$$u_{EO}(r,z) \approx \partial_z \psi_{appl} \frac{\varepsilon_0 \varepsilon_r}{\eta}(\psi - \psi_0), \tag{93}$$

where ψ_0 is a known constant. The pressure-induced flux is given by

$$\begin{aligned} J_{adv,p} &= 2\pi \int_0^R r(\rho_s - 2\bar{\rho}_s) u_p dr \\ &= -\pi \frac{\partial_z p}{2\eta} \int_0^R r(\rho_s(r,z) - 2\rho_b)(R(z)^2 - r^2). \end{aligned} \tag{94}$$

Using $\rho_s(r,z) = 2\bar{\rho}_s(z)\cosh[\phi(r)]$, we find

$$\begin{aligned} J_{adv,p} &= -\frac{\partial_z p}{4\eta}\left(2\bar{\rho}_s\int_0^R r(\cosh(\phi)(R^2-r^2)dr - 2\rho_b\int_0^R r(R^2-r^2)\right) \\ &= -\frac{\pi\partial_z p}{\eta}\left(\frac{1}{4}R^4(\bar{\rho}_s-\rho_b) + \bar{\rho}_s\int_0^R r(\cosh(\phi-1)(R^2-r^2)dr\right). \end{aligned} \tag{95}$$

The integrand is only non-zero in the EDL, so we can transform it such that it is a function of the s coordinate, where $s \equiv R - r$. The term $R^2 - r^2$ can be written as $(R-r)(R+r) = s(2R-s)$, so

$$J_{adv,p} = -\frac{\pi\partial_z p}{\eta}R(z)\bar{\rho}_s\left(\frac{R^3}{4}(1-\frac{\rho_b}{\bar{\rho}_s}) + 2R(z)\int_0^R s(\cosh(\phi)-1)ds - \int_0^R s^2(\cosh(\phi)-1)ds\right). \tag{96}$$

Here we recognize two other PB integrals as defined by Werkhoven [6]:

$$P_3 = \frac{1}{\bar{\lambda}_D^2}\int_0^R dss(\cosh(\phi)-1), \tag{97}$$

$$P_4 = \frac{1}{\bar{\lambda}_D^3}\int_0^R dss^2(\cosh(\phi)-1). \tag{98}$$

So

$$J_{adv,p} = -\frac{\pi\partial_z p}{\eta}R(z)\bar{\lambda}_D^2\bar{\rho}_s\left(\frac{R^3}{4\lambda_D^2}(1-\frac{\rho_b}{\bar{\rho}_s}) + 2R(z)P_3 - \bar{\lambda}_D P_4\right). \tag{99}$$

Similarly, the electro-osmotic contribution is given by

$$\begin{aligned} J_{adv,EO} &= 2\pi\partial_z\psi_{appl}\frac{\varepsilon_0\varepsilon_r}{e\eta\beta}\int_0^R r(\rho_s - 2\rho_b)(\phi-\phi_0) \\ &= 2\pi\partial_z\psi_{appl}\frac{\varepsilon_0\varepsilon_r}{e\eta\beta}\left(2\bar{\rho}_s R(z)\int_0^R ds(\cosh(\phi)-1)(\phi-\phi_0) + (\bar{\rho}_s-\rho_b)\int_0^R drr(\phi-\phi_0)\right) \\ &= \frac{4\pi\varepsilon_0\varepsilon_r}{e\eta\beta}R(z)P_5\bar{\rho}_s\partial_z\psi_{appl}\left(\bar{\lambda}_D P_5 + (1-\frac{\rho_b}{\bar{\rho}_s})(\bar{\lambda}_D P_1 - \frac{1}{2}\phi_0 R)\right), \end{aligned} \tag{100}$$

where P_5 is given by: [6]

$$P_5 = \frac{1}{\bar{\lambda}_D}\int_0^R ds(\cosh(\phi)-1)(\phi-\phi_0). \tag{101}$$

We now have analytical expressions for all the contributions to the excess flux. We can recall from section 4 that $P_1 = 1.50784$ and $P_2 = 0.638373$. Similarly we can also calculate the values for the other Poisson-Boltzmann integrals and find $P_3 = 0.296138$, $P_4 = 0.285357$ and $P_5 = 0.325015$, for these values of σ and ρ_b as stated in section 4. To simplify the expressions for the advective fluxes of equations 99 and 100 we now switch to the total flux instead of the excess flux. Note that this is not the flux that could be calculated with a symmetric Onsager-like matrix. We have numerical solutions for this system so it is easy to compare the order of magnitude of the various contributions. A few approximations can be made; the terms in the streaming flux $I_{adv,p}$ that depend on RP_3 and $\lambda_D P_4$ are much smaller than the term that goes with $R^3/(4\lambda_D^2)$, so they can safely be ignored. The term that goes with $\lambda_D P_5$ in the electro-osmotic advective current $I_{adv,EO}$ can also safely be ignored. The term $\lambda_D P_1$, however, is roughly a factor 5 larger and cannot be ignored. The space charge ρ_e^{sp} is also too small to make a significant contribution. Collecting all the contributions and making these approximations we get:

$$J_{cond} = 2\pi Re\beta D\sigma(\partial_z\psi_{appl}), \tag{102}$$

$$J_{diff} = -\pi R^2 D(\partial_z \bar{\rho}_s), \tag{103}$$

$$J_{adv,p} = -\frac{\partial_z p}{4\eta}\pi R^4 \bar{\rho}_s, \tag{104}$$

$$J_{adv,EO} = -\frac{e\partial_z \psi_{appl}}{\eta \lambda_B}\bar{\lambda}_D R\left(P_1 - \frac{R}{2\bar{\lambda}_D}\phi_0\right)\bar{\rho}_s. \tag{105}$$

Note that the approximations that we made to the advective salt fluxes can be interpreted as ignoring the salt flux through the electric double layer since equations 104 and 105 can be simplified by writing it in terms of the volume flux through the channel:

$$J_{adv} = J_{adv,p} + J_{adv,EO} = 2Q_{tot}\bar{\rho}_s, \tag{106}$$

where we recognized that

$$Q_{tot} = Q_{str} + Q_{EO} = -\frac{\partial_z p}{8\eta}\pi R^4 - \frac{e\partial_z \psi_{appl}}{2\eta\lambda_B}\bar{\lambda}_D R\left(P_1 - \frac{R}{2\bar{\lambda}_D}\phi_0\right) \tag{107}$$

and where Q_{str} is the streaming volume flux due to the pressure gradient and Q_{EO} is the electro-osmotic volume flux, due tot the electric field.

When we derived the Stokes equations from the Navier-Stokes equation in section 3, we used a non-dimensional parameter, the Reynolds number Re, to determine whether the inertial or the viscous forces dominated for a certain fluid velocity and geometry. Here we can do something similar. Without going into detail about the non-dimensional Nernst-Planck equation, we can identify a non-dimensional parameter, the Peclét number Pe, which determines the relative importance of diffusive and advective ion fluxes. We define the Peclét number as $\mathrm{Pe} = R_0\bar{u}/D$, where $\bar{u}$ is a characteristic average velocity in the channel and R_0 is a characteristic length scale of our system, for which we took the radius at the tip. In terms of volume fluxes, we could write this as $\mathrm{Pe} = \frac{Q}{\pi R_0 D}$, where we used the average velocity at the tip of the cone $\bar{u} = Q/(\pi R_0^2)$ as a characteristic velocity.

The diffusive term can be ignored in the high Peclét regime. This seems to be the case for the solution where $\Delta V = 400$mV. The system is in the high Peclét regime regardless of the applied pressure Δp because the pressure works in the same direction as the electro-osmotic flow for ΔV. For $\Delta V = 400$ mV and $\Delta p = 0$, Q is in the order of magnitude of 10^{-15} m^3/s, which corresponds to $\mathrm{Pe} \approx 3$. Increasing Δp only increases Pe in this case. For negative ΔV, however, we must be careful since the pressure gradient and the electrical potential gradient have opposite signs. This means that Q, and therefore Pe, passes through zero when Δp increases, and we cannot make this approximation.

6.3.1 High Peclét Number

In the high Peclét regime we can therefore say that:

$$J_{tot} = 2\pi R D\sigma(\partial_z \phi_{appl}) + 2\bar{\rho}_s\left(Q_{str} + Q_{EO}\right). \tag{108}$$

We require the total salt flux to be constant throughout the channel, *i.e.* $\partial_z J_{tot} = 0$. This yields an inhomogeneous first order differential equation. Our approximate expressions for the flow profile may yield a volume flux Q that is not divergence free due to the number of approximation we made, but in reality any solution of the Stokes equation for non-compressible fluids should be divergence free. Therefore we should ignore any z-dependence in Q_{tot}, since this is only an artifact of the approximations. We known that

$$\phi_{appl}(z) = \frac{\ell - z}{\ell}\frac{R_0 + R_d}{R(z)}(e\beta\Delta V) \tag{109}$$

and

$$R(z) = R_0 + R_{dev}(1 - \frac{z}{\ell}) = R_0 + a(\ell - z), \tag{110}$$

where $a = R_{dev}/\ell$ is the slope of the cone and where we chose the origin of our coordinate system to be at the wide end of the cone. Differentiating J_{tot} and requiring the derivative to be zero yields the equation

$$\partial_z J_{tot} = 2\pi D\sigma(e\beta\Delta V)\frac{\partial}{\partial z}\left(R(z)\partial_z\left(\frac{\ell - z}{\ell}\frac{R(0)}{R(z)}\right)\right) + 2Q_{tot}(\partial_z\bar{\rho}_s) = 0 \tag{111}$$

When we apply the boundary condition that $\bar{\rho}_s(0) = \rho_b$, we find an analytical solution to the equation $\partial_z J_{tot} = 0$:

$$\bar{\rho}_s(z) = \rho_b + \frac{z}{R(z)}\frac{\pi R_0 R_d D\sigma}{\ell^2 Q_{tot}}(e\beta\Delta V) \tag{112}$$

The conduction current that would result from this concentration profile is given by

$$\begin{aligned} I_{cond} &= -2\pi e^2\beta D(\partial_z\psi_{appl})\int_0^R drr\rho_s(r,z) \\ &= -4\pi eD(\partial_z\phi_{appl})\bar{\rho}_s(z)\int_0^R drr\cosh(\phi) \\ &= -4\pi eD(\partial_z\phi_{appl})\left(\rho_b + \frac{z}{R(z)}\frac{\pi R_0 R_d D\sigma}{\ell^2 Q}(e\beta\Delta V)\right)\left(\lambda_D R P_2 + \frac{1}{2}R^2\right). \end{aligned} \tag{113}$$

6.3.2 Low Peclét Number

In the low Peclét regime we cannot ignore the diffusive flux. In the cases that we are interested in, we also cannot consider Pe to be so small that we can ignore the the advective fluxes altogether, since we are interested in the response of the current to driving forces. We would have to solve $\partial_z J_{tot} = 0$ with the full expression for J_{tot}:

$$J_{tot} = 2\pi RD\sigma(\partial_z\phi_{appl}) - \pi R^2 D(\partial_z\bar{\rho}_s) + 2Q\bar{\rho}_s. \tag{114}$$

This yields an inhomogeneous second order differential equation. There may be analytical solutions to this equation, but for convenience we choose to focus on the simpler case $\Delta V = 400$ mV where the system is firmly situated in the high Peclét number regime .

7 Results

In the previous section we derived an expression for the salt concentration profile, and the resulting conduction current for high Peclét number. The analytical expression for the concentrations profile from equation 112 is shown in figure 17. When we compare this to the numerical COMSOL concentration profile from figure 14, we see that the profiles agree quite well, qualitatively. We see that ion depletion is not as strong in the analytical expression as it was in the COMSOL calculations. The fact that we observe a deviation from the numerical data is perhaps not entirely unexpected considering the amount of approximations we made. Note that the difference between concentration profiles decreases non-linearly with an increasing pressure difference, similarly to the numerical solution, but that the relative distance between the concentration is lower. As such, we expect its corresponding conduction current to exhibit less non-linear behavior.

We can now plot the analytical conduction current from equation 113. We expect the conductivity of the analytical expression to be higher than the numerical data, since the analytical ion depletion is less strong. Both the numeral and the analytical conduction currents, the former being radially integrated at $z = 2\ell/3$, are shown in figure 18. We can see the transistor-like behavior described by Jubin [8], albeit less pronounced than in the numerical simulation.

Technically, ion accumulation or depletion could influence the streaming current too, since the Debye length λ_D depends on $\sqrt{\rho_s}$ and the flow profile is not constant as a function of r, but this effect will be negligible.This was confirmed by the numerical data, as shown in figure 13 where the streaming current was linear in Δp. We can therefore approximate the streaming current with equation 43 for the streaming current in a cylinder with the substitution $R \to R(z)$. We can then plot the total pressure-induced current, as shown in figure 19. We do see non-linear behavior in the analytical current response but it is not as strong an effect as we see in the COMSOL simulations. It seems, however, as if most of the discrepancy between the two solutions lies in the approximation for the volume flux Q. We did not take any of the fluid mechanics that is specific to the cone into account for the derivation of the salt flux. Our analytical expression for the volume flux, equation 107, and the numerical calculation are shown in figure 20, and we see that the solutions can differ by as much as 30%. The total current response where the numerical values for Q were used in the analytical expression for the conduction current is shown in figure 21, and it agrees perfectly with the simulation. This proves that equation 113 fully captures the non-linear current responses.

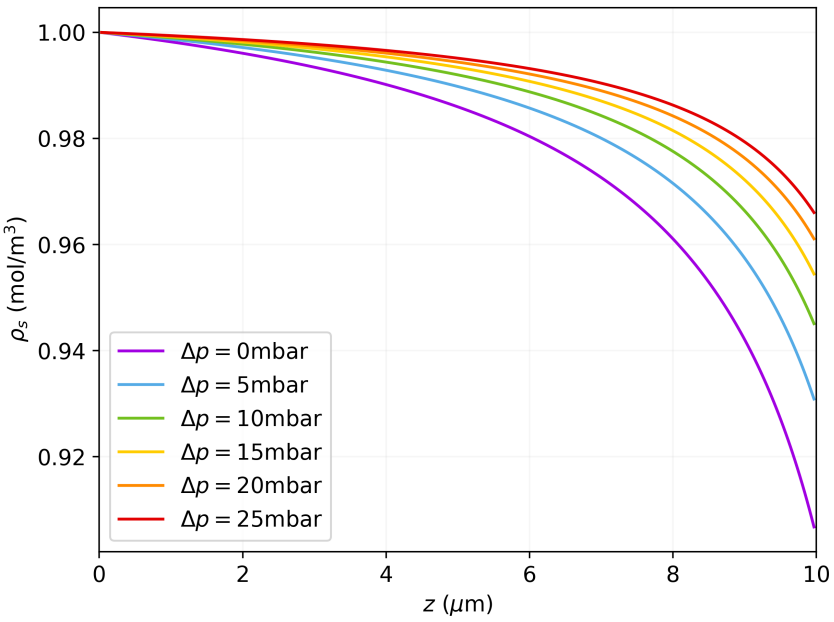

Figure 17: Theoretical concentration profiles given by equation 112 at ΔV for different values of Δp

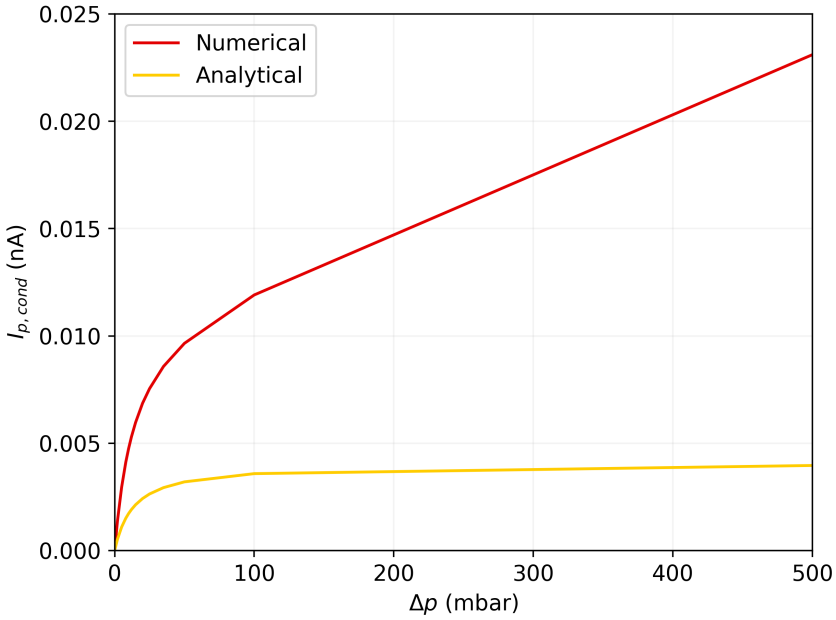

Figure 18: Both the numerical and fully analytical pressure-induced conduction current (equation 113) at $\Delta V = 400\text{mV}$

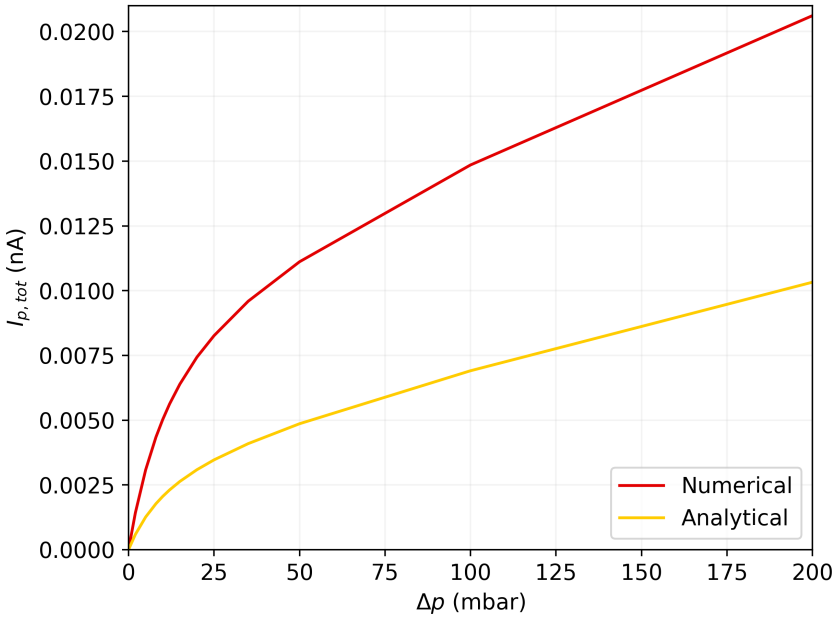

Figure 19: Total pressure-induced currents, both analytical and numerical, at $\Delta V = 400\text{mV}$

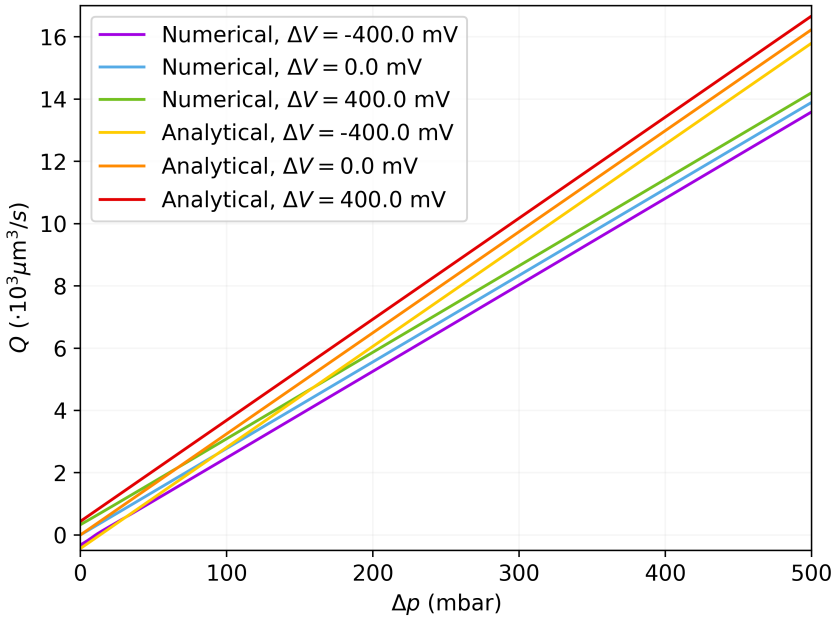

Figure 20: Analytical and numerical volume flux Q_{tot} at $\Delta V = 400$ mV as a function of Δp

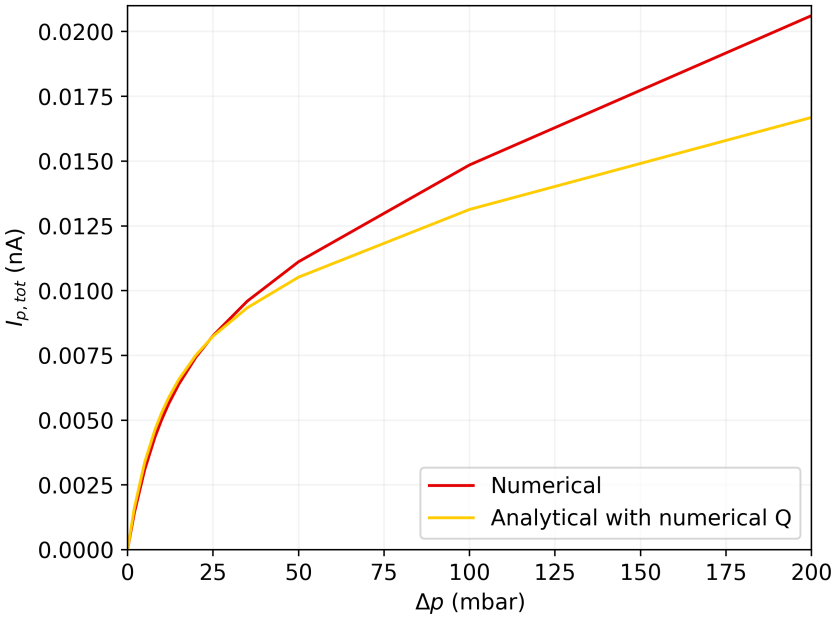

Figure 21: Total numerical current and analytical expression (equations 113 and 43) for the current, where the numerical values for Q were used in the analytical expression for the conduction current.

The fact that the total salt flux must be constant in a channel where the radius is not constant induces ion depletion. The dependence of the ion depletion on the streaming volume flux Q, combined with the fact that the conduction current is dependent on the salt concentration, causes a transistor-like behavior.

Interestingly enough, there have been studies that numerically investigated the effect of pressure on ion depletion or accumulation. [21] [26]. These were done in the context of current rectification and studied the $I-V$ curve when a fixed pressure difference was applied. Lan *et al* noticed that the dependence of the ion depletion on the pressure difference was dependent on the radius of the tip of the cone. Ion concentrations did not seem to be affected by a pressure difference when they simulated a cone with a tip that has a radius of 35nm, whereas they found a strong correlation for a cone with a minimal radius of 185nm. In our theoretical description, this can be rationalized with the fact that the streaming volume flux Q_{str} goes with R^4 while the electro-osmotic volume flux Q_{EO} depends on R^2. Electrical driving is much more efficient in small channels than hydraulic driving, so the pressure-induced fluid flow is negligible in nanometer-scale channels. We therefore expect the non-linear current response to 'flatten' when the radius of the channel is decreased. Furthermore, we expect there to be a maximum since at large R_0 the conductive salt flux must be small compared to the advective flux. To study the dependence of the non-linearity of the current response on the radius of the tip, R_0, we introduce a parameter t_r, which is the ratio between the slope of the current response at $\Delta p = 0$ and $\Delta p = 500$mbar.

$$t_R = \frac{\partial_p I_p|_{p=0\text{mbar}}}{\partial_p I_p|_{p=500\text{mbar}}} \tag{115}$$

We can plot this parameter as a function of R_0, as shown in figure 22 and see a maximum in t_R at around 260nm. This can be used to design nanopores of which the conduction current can be tuned more precisely. Note that equation 111 is a general equation for the salt flux in the high Peclét regime, that is not limited to conical geometries. As such, it can be used to describe the ion depletion in a variety of geometries and is not limited to conical nanopores. We did make a small angle approximation $a \ll 1$, where a is the slope of the cone. In a general geometry, this would be equivalent to saying that the slope at any height z of the geometry is small. There may not be analytical solutions to this equation for any geometry parameterized by a function $R(z)$, but it still may be used on similarly simple geometries.

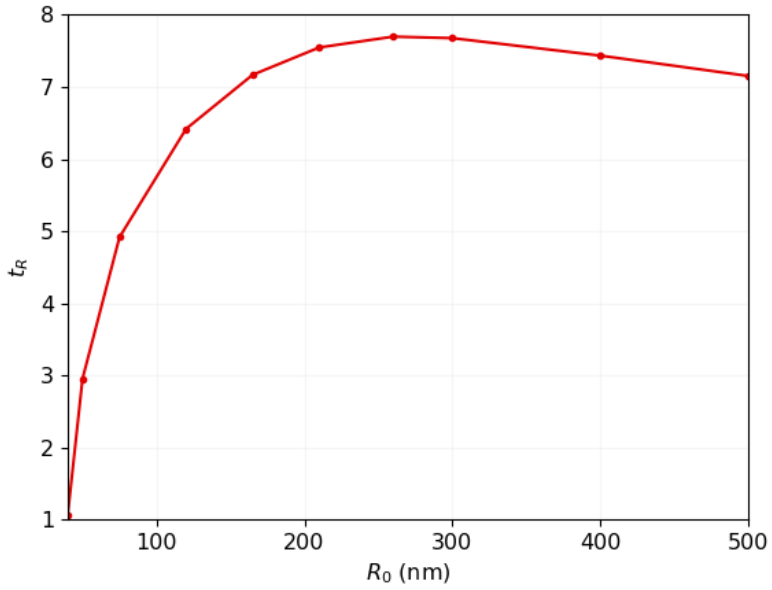

Figure 22: Numerically determined t_R as a function of R_0, for $\Delta V = 400$ mV

8 Discussion

This research project set out to investigate the transistor-like behavior of conical nanochannels under a combination of hydraulic and electric driving forces that was reported by Jubin *et al.* [8]. Analysis of the numerical data that was generated with the finite elements software COMSOL pointed towards the conduction current as the source of this non-linear current response. We then studied the salt flux in a cone and found an analytical expression for the salt concentration, which causes the conduction current. With this we successfully recovered a non-linear current response that was similar to the experimental observations of Jubin *et al.* [8].

Our approach for the explanation of the phenomenon differs from that of Jubin *et al.*. They put forth a model with so-called Spatially Charged Zones, a space charge outside of the electric double layer. They show numerically that solving the PNPS equations while allowing SCZs to exist could lead to the observed non-linear current. We on the other hand focused on the salt concentration profile in the channel, where we observed a strong ion depletion for low values of Δp. This shift of focus towards salt concentrations can be rationalized with the results of numerical simulations. We did observe a space charge outside of the EDL, but this charge was roughly five orders of magnitude smaller than the charge inside the EDL ($\sim 10^0$ C/m^3 versus $\sim 10^5$ C/m^3 in the EDL). It seems highly unlikely that this plays an important role. This is further supported by data from COMSOL, with which it is possible to discern the different contributions to the total current. The data shows that the streaming current was completely linear in Δp, also suggesting that SCZs do not play a large role in the currents. The numerical results of Jubin ET AL. do not necessarily contradict ours, however, since they numerically solved the full set of PNPS equations. This automatically captures the ion depletion effect, as shown in figure S3 of the supplemental materials of the paper [8], and therefore also the non-linear conduction current.

The analytical theory we developed was based on a number of approximations, some of which are limiting its generalizability. For $\Delta V = -400$ mV, for instance, we could not determine the current response due to the fact that the system passed through a region of very low Peclét number, in which the approximation that the diffusive salt flux was negligible was not valid. This is unfortunate since there we saw an interesting current response for low Δp in our numerical data. The analytical theory is also limited in applicability by some rather crude approximations, that threw out some of the more subtle physics phenomena too like ion current rectification. It does fully capture the non-linear current response, but our approximation for the volume flux Q in a cone was not very accurate, making the analytical expression for the conduction current quantitatively deviate from the numerical data. Phenomenologically speaking, however, we did show that the ion depletion in the channel was the mechanism that was responsible for the non-linear current. It would be interesting to further analyze all the approximations that we made to see if we can find a more complex expression for the current that would also capture ionic current rectification.

The occurrence of ion depletion in conical nanochannels, and the influence of the pressure thereon have been observed before [26] [21] [22], but this has, as far as we know, never been linked to the non-linear pressure-induced currents that were described by Jubin *et al.*. Ion depletion does not only happen in conical geometries, however, and is also expected in channels with other shapes. It would be interesting to investigate the influence of the specific geometry on the non-linearity of the current. New types of nanochannels could be designed to maximize the transistor-like behaviour of the channel, allowing for a greater adjustability in sensitivity to an external electric field. This could possibly find application in tunable blue (osmotic) energy conversion.[8] Further research would need to be conducted on the influence of conicity on diffusioosmosis. It would be interesting to see how the diffusioosmotic force couples with the hydraulic and electric driving forces and how it would influence the concentration profile in the channel.

9 Conclusions

This thesis aimed to explain from first principles the non-linearity in the current that was experimentally observed by Jubin *et al.*.[8] They reported a strong increase in conductivity when a pressure difference was applied over a conical nanopore, in the presence of a fixed electric field. We have shown that this phenomenon is caused by a depletion of ions in the channel, as opposed to the previously accepted theory that was proposed by Jubin *et al.*. They argued that a space charge outside of the EDL was the cause of a non-linear current, but we showed numerically that the magnitude of this charge was so small that any contributions to the current are negligible.

When an electric field is applied, without a pressure difference, the salt concentration profile in the channel decreases or increases depending on the sign of the electric field. We show that this is required by a conservation of salt flux through the channel. The different contributions to the salt flux must add up to a constant total flux for every 'slice' of the channel, even when the radius of the channel is non-homogeneous. This can only be achieved when the concentration decreases or increases at the tip of the channel. We derived analytical expression for the salt concentration profiles and the corresponding conduction current, using a Poisson-Boltzmann formalism for the EDL, and showed that they lead to a non-linear pressure-induced current in a conical geometry.

References

[1] M. Queralt-Martín et al. "Electrical pumping of potassium ions against an external concentration gradient in a biological ion channel". In: *Applied Physics Letters* 103.4 (2013). DOI: 10.1063/1.4816748.

[2] B. Hille. "Ionic channels in excitable membranes. Current problems and biophysical approaches". In: *Biophysical Journal* 22.2 (1978), pp. 283–294. DOI: 10.1016/S0006-3495(78)85489-7.

[3] R. B. Schoch, J. Han, and P. Renaud. "Transport phenomena in nanofluidics". In: *Rev. Mod. Phys.* 80 (3 2008), pp. 839–883. DOI: 10.1103/RevModPhys.80.839.

[4] R.E. Pattle. "Production of electric power by mixing fresh and salt water in the hydroelectric pile [19]". In: *Nature* 174.4431 (1954), p. 660. DOI: 10.1038/174660a0.

[5] Z. Jia et al. "Blue energy: Current technologies for sustainable power generation from water salinity gradient". In: *Renewable and Sustainable Energy Reviews* 31 (2014), pp. 91–100. DOI: 10.1016/j.rser.2013.11.049.

[6] B.L. Werkhoven and R. Van Roij. "Coupled water, charge and salt transport in heterogeneous nanofluidic systems". In: *Soft Matter* 16.6 (2020), pp. 1527–1537. DOI: 10.1039/c9sm02144b.

[7] R. van Roij. "Soft Condensed Matter Theory". Utrecht University, 2018.

[8] L. Jubin et al. "Dramatic pressure-sensitive ion conduction in conical nanopores". In: *Proceedings of the National Academy of Sciences* 115.16 (2018), pp. 4063–4068. DOI: 10.1073/pnas.1721987115.

[9] P. C. Hiemenz and R. Rajagopalan. *Principles of Colloid and Surface Chemistry, 3rd ed., rev. and expanded*. Marcel Dekker, Inc, 1997. ISBN: 0824793978.

[10] H.J. Butt, K. Graf, and M. Kappl. *Physics and Chemistry of Interfaces*. Wiley-VCH GmbH & Co. KGaA, 2003. ISBN: 9783527404131.

[11] C.L. Rice and R. Whitehead. "Electrokinetic Flow in a Narrow Cylindrical Capillary". In: *The Journal of Physical Chemistry* 69.11 (1965), pp. 4017–4023. DOI: https://doi.org/10.1021/j100895a062.

[12] *NIST Digital Library of Mathematical Functions*. http://dlmf.nist.gov/, Release 1.0.25 of 2019-12-15. F. W. J. Olver, A. B. Olde Daalhuis, D. W. Lozier, B. I. Schneider, R. F. Boisvert, C. W. Clark, B. R. Miller, B. V. Saunders, H. S. Cohl, and M. A. McClain, eds. URL: http://dlmf.nist.gov/.

[13] B.L. Werkhoven. "Static and Dynamic Solid-Water Interfaces. Charge regulation, diffusio-osmosis and inhomogeneous electrokinetics". Doctoral dissertation. Utrecht University, 2020.

[14] B. J. Kirby. *Micro- and Nanoscale Fluid Mechanics. Transport in Microfluidic Devices*. Cornell University: Cambridge University Press, 2010. ISBN: 978-0-521-11903-0.

[15] L. Onsager. "Reciprocal relations in irreversible processes. II". In: *Physical Review* 38.12 (1931), pp. 2265–2279. DOI: 10.1103/PhysRev.38.2265.

[16] P. B. Peters et al. "Analysis of electrolyte transport through charged nanopores". In: *Phys. Rev. E* 93 (5 2016), p. 053108. DOI: 10.1103/PhysRevE.93.053108.

[17] C G Gray and P J Stiles. "Nonlinear electrostatics: the Poisson–Boltzmann equation". In: *European Journal of Physics* 39.5 (2018). DOI: 10.1088/1361-6404/aaca5a.

[18] H.D. Young and R.A. Freedman. *University Physics. with Modern Physics*. 14th ed. Pearson, p. 822.

[19] Z.S. Siwy. "Ion-current rectification in nanopores and nanotubes with broken symmetry". In: 16.6 (2006), pp. 735–746. DOI: 10.1002/adfm.200500471.

[20] K. Zhou, J.M. Perry, and S.C. Jacobson. "Transport and sensing in nanofluidic devices". In: 4 (2011), pp. 321–341. DOI: 10.1146/annurev-anchem-061010-113938.

[21] W.-J. Lan, D.A. Holden, and H.S. White. "Pressure-dependent ion current rectification in conical-shaped glass nanopores". In: 133.34 (2011), pp. 13300–13303. DOI: 10.1021/ja205773a.

[22] W.-J. Lan et al. "Voltage-Rectified Current and Fluid Flow in Conical Nanopores". In: 49.11 (2016), pp. 2605–2613. DOI: 10.1021/acs.accounts.6b00395.

[23] Myung-Suk Chun, Sang-Yup Lee, and Seung-Man Yang. "Estimation of zeta potential by electrokinetic analysis of ionic fluid flows through a divergent microchannel". In: *Journal of colloid and interface science* 266 (2003), pp. 120–6. DOI: 10.1016/S0021-9797(03)00576-9.

[24] J. Happel and H Brenner. *Low Reynolds number hydrodynamics*. Martinus Nijhoff Publishers, The Hague, 1983. Chap. 4.24. ISBN: 978-90-247-2877-0. DOI: 10.1007/978-94-009-8352-6.

[25] S. Ghosal. "Fluid mechanics of electroosmotic flow and its effect on band broadening in capillary electrophoresis". In: 25.2 (2004), pp. 214–228. DOI: 10.1002/elps.200305745.

[26] F. Qian et al. "Electrokinetic power generation in conical nanochannels: Regulation effects due to conicity". In: 22.4 (2020), pp. 2386–2398. DOI: 10.1039/c9cp05317d.